Miocene extension in the East Range, Nevada: A two-stage history of normal faulting in the northern Basin and Range

J.C. Fosdick†
J.P. Colgan*
Department of Geological and Environmental Sciences, Stanford University, Stanford, California 94305, USA

ABSTRACT

The East Range in northwestern Nevada is a large, east-tilted crustal block bounded by west-dipping normal faults. Detailed mapping of Tertiary stratigraphic units demonstrates a two-phase history of faulting and extension. The oldest sedimentary and volcanic rocks in the area record cumulative tilting of ~30°–45°E, whereas younger olivine basalt flows indicate only a 15°–20°E tilt since ca. 17–13 Ma. Cumulative fault slip during these two episodes caused a minimum of 40% extensional strain across the East Range, and Quaternary fault scarps and seismic activity indicate that fault motion has continued to the present day. Apatite fission track and (U-Th)/He data presented here show that faulting began in the East Range ca. 17–15 Ma, coeval with middle Miocene extension that occurred across much of the Basin and Range. This phase of extension occurred contemporaneously with middle Miocene volcanism related to the nearby northern Nevada rifts, suggesting a link between magmatism and extensional stresses in the crust that facilitated normal faulting in the East Range.

Younger fault slip, although less well constrained, began after 10 Ma and is synchronous with the onset of low-magnitude extension in many parts of northwestern Nevada and eastern California. These findings imply that, rather than migrating west across a discrete boundary, late Miocene extension in western Nevada is a distinct, younger period of faulting that is superimposed on the older, middle Miocene distribution of extended and unextended domains. The partitioning of such middle Miocene deformation may reflect the influence of localized heterogeneities in crustal structure, whereas the more broadly distributed late Miocene extension may reflect a stronger influence from regional plate boundary processes that began in the late Miocene.

Keywords: Basin and Range, East Range, U-Th/He thermochronology, fission track, magmatism, extension.

INTRODUCTION

Although early Tertiary extension took place along the eastern margin of the northern Basin and Range (McGrew et al., 2000; Rahl et al., 2002; Wells et al., 2000; Egger et al., 2003) (Fig. 1), the main phase of extension across much of the province began in the middle Miocene. A broad region, encompassing much of central and southern Nevada and parts of southeastern California, underwent extensional faulting beginning ca. 17–15 Ma (Proffett, 1977; Dilles and Gans, 1995; Faulds et al., 2005; Miller et al., 1999; Snow and Wernicke, 2000; Stockli et al., 2002; Stockli, 2005; Colgan et al., 2008). The spatial distribution of strain during this period was strongly heterogeneous, with highly extended domains (up to 100% strain or more) separated by relatively undeformed blocks of crust (e.g., Miller et al., 1999; Hudson et al., 2000). In contrast, a large area of western and northwestern Nevada remained essentially undeformed until ca. 12–10 Ma (e.g., Colgan et al., 2006a; Stockli et al., 2003; Henry and Perkins, 2001). Subsequent faulting in this region took place on widely spaced high angle faults that accommodated much less strain (~15%–20%) (Colgan et al., 2006b; Lerch et al., 2006) than that documented in the highly extended middle Miocene domains in central and southern Nevada. The goal of this study is to investigate the location and nature of the boundary—if one exists—between low-magnitude, late Miocene extension in northwestern Nevada and the large region of Nevada affected by significant middle Miocene extension.

The East Range and Sou Hills (Fig. 1) lie south and east of the area where extensional faulting is known to have begun in the late Miocene, and north and west of moderately to highly extended regions like the Stillwater Range (Hudson et al., 2000) and the Shoshone and northern Toiyabe Ranges (Smith et al., 1991; Colgan et al., 2008) (Fig. 1). Together, the East Range and Sou Hills expose tilted Oligocene to Miocene sedimentary and volcanic rocks that record the magnitude and overall timing of extensional faulting. Furthermore, the East Range exposes an ~8 km structural section across an Oligocene pluton exhumed in the footwall of a large normal fault (Fig. 2), making it an ideal location for direct dating of extension using low-temperature thermochronology.

Apatite fission track and (U-Th)/He data from the East Range, coupled with detailed mapping of the Tertiary stratigraphy in the nearby Sou Hills, reveal a two-phase history of faulting and crustal extension, with an initial event at 17–15 Ma, followed by a distinctly younger period of faulting that is poorly constrained but younger than 10 Ma. This result suggests that, rather than migrating west across a discrete boundary, late Miocene extension in western Nevada is a distinct, younger period of faulting that is superimposed on the older, middle Miocene pattern of extended and unextended domains.

REGIONAL SETTING

The East Range lies in the northern Basin and Range extensional province and was exhumed in the footwall of a west-dipping fault system that accommodated eastward tilting of Cenozoic strata and unroofing of pre-Cenozoic basement (Figs. 1 and 2). Quaternary fault scarps and geothermal springs along the western flank of the East Range indicate recent faulting (Wallace, 1984). The East Range is east of the Walker Lane (Stewart, 1980) (Fig. 1), a zone of dextral faults in the northwestern Great Basin that accommodates nearly 15%–25% of the Pacific–North

†E-mail: julief@stanford.edu
*Present address: U.S. Geological Survey, Menlo Park, California 94025, USA

GSA Bulletin; September/October 2008; v. 120; no. 9/10; p. 1198–1213; doi: 10.1130/B26201.1; 9 figures; 1 table; Data Repository item 2008066.

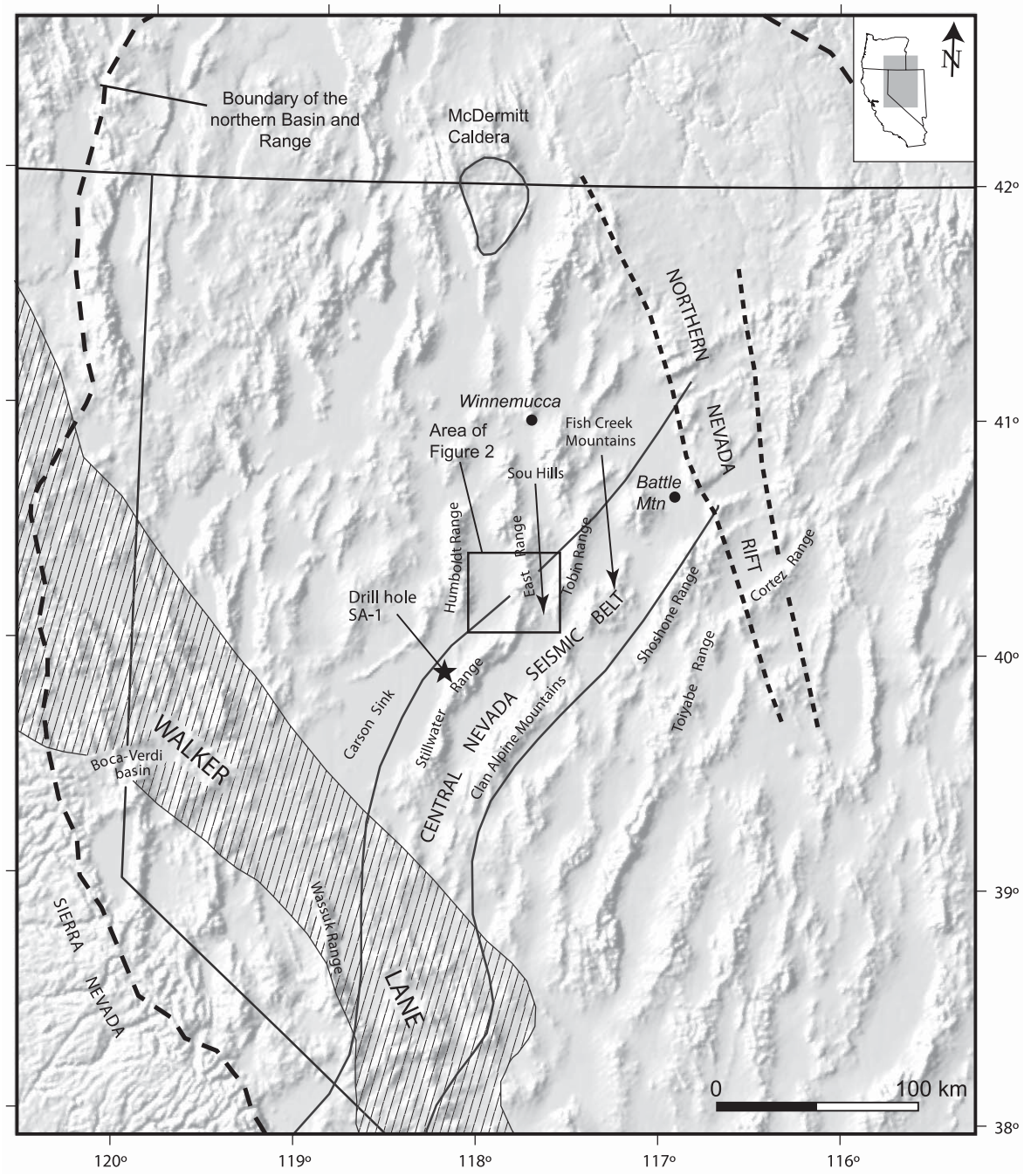

Figure 1. Shaded relief map of the northwestern part of the northern Basin and Range Province, showing geographic features discussed in text. Locations of the Walker Lane from Faulds et al. (2005) and references therein, the Northern Nevada Rift from aeromagnetic lineations (Zoback et al., 1994; Glen and Ponce, 2002), and the Central Nevada Seismic Belt from Wallace (1984). Base map modified from NOAA 90 s digital elevation data. Refer to text for references. Drill hole SA-1 location of Hastings (1979).

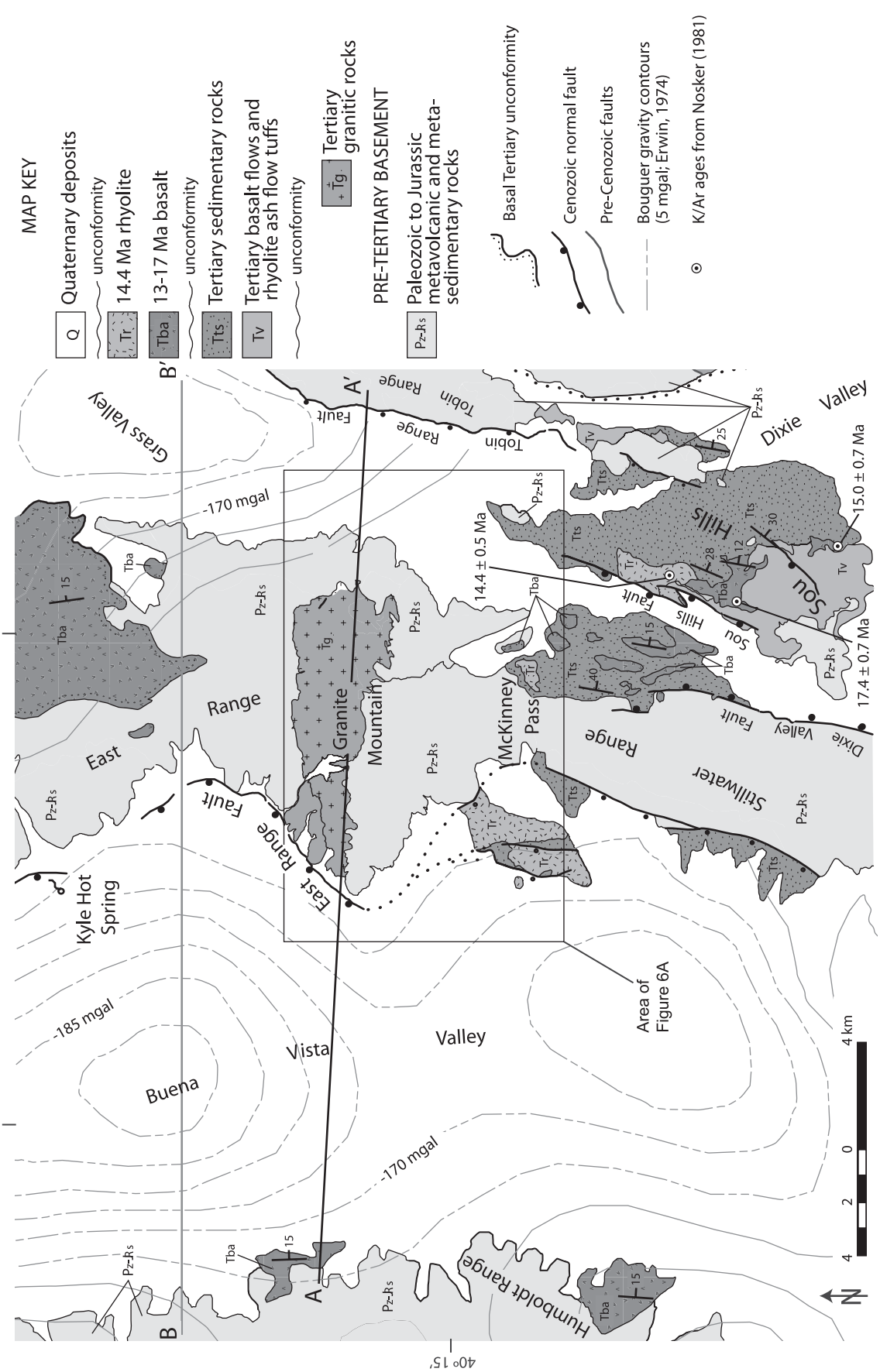

Figure 2. Generalized geologic map of the East Range (compiled from Stewart and Carlson, 1978), with additions and changes based on new mapping by the authors. Bouguer gravity anomalies are shown in dashed black lines in 5 mgal contours (from Erwin, 1974), also portrayed in cross section B–B′ in Figure 5. Previously published K/Ar ages of volcanic rocks in the Sou Hills are from Nosker (1981).

American plate motion. At the latitude of the study area, initiation of strike-slip faulting within the Walker Lane began ca. 9 Ma and continued into the Holocene (e.g., Dilles and Gans, 1995; Faulds et al., 2005). Additionally, the study area lies within the Central Nevada Seismic Belt, a region of significant seismic activity. The surface rupture of the 1915 Pleasant Valley earthquake (**M** 7.1) lies just to the north, and the 1954 Dixie Valley surface ruptures (**M** 7.2 and 6.8) are just to the south (e.g., Wallace, 1984; Caskey et al., 2000) (Fig. 2).

Global Positioning System (GPS) measurements across the northern Basin and Range show a total of 2.8 ± 0.2 mm/yr of diffuse E-W extension occurring today across the entire Great Basin between the Sierra Nevada and Colorado Plateau (Fig. 1), but higher strain rates are observed within the Central Nevada Seismic Belt in comparison with central Nevada (Bennett et al., 2003).

GEOLOGY OF THE EAST RANGE AND SOU HILLS

Pre-Cenozoic basement rocks in the East Range (Fig. 2) consist of (1) upper Paleozoic basinal quartzite, chert, argillite, and sandstone of the Havallah sequence; (2) Permian–Triassic mafic to felsic volcanic rocks and shallow intrusive rocks of the Koipato Group, and (3) Triassic to Early Jurassic marine limestone and shale of the Star Peak and Auld Lang Syne Groups (e.g., Nichols and Silberling, 1977). Compressional deformation during the Permian–Triassic Sonoma orogeny resulted in complex folding and eastward thrusting of the Havallah sequence over contemporaneous shelf facies along the Golconda Thrust (Silberling, 1975; Burke, 1977). Folded Paleozoic and Mesozoic strata are now exposed in the northern Stillwater Range and underlie Tertiary strata across the field area at McKinney Pass, the Sou Hills, and the southwestern Tobin Range (Fig. 2).

Cenozoic Units

Cenozoic rocks in the East Range and Sou Hills consist of Oligocene granitic and dioritic plutons, gabbroic dikes, Oligocene–Miocene rhyolite ash-flow tuff, tuffaceous sediments, basalt flows, and rhyolite lava flows and plugs (Fosdick, 2006) (Figs. 2 and 3). Geologic mapping, compiled with previous mapping by Burke (1977), Stewart and Carlson (1978), and Nosker (1981), establish that Oligocene(?) to Pliocene sedimentary and volcanic strata unconformably overlie the pre-Cenozoic basement or are in normal fault contact with basement rocks (Fig. 3). Up to 1500 m of continuous sedimentary and volcanic section is uplifted and exposed in the central Sou Hills. This stratigraphic section has a maximum composite thickness of nearly 2900 m and is summarized with reported ages in Figure 3 with detailed descriptions in Fosdick (2006).

Oligocene Plutonic Complex

At Granite Mountain in the southern East Range a Tertiary plutonic complex intrudes Paleozoic and Triassic basement (Fig. 2). Mapping of the Tertiary pluton by Whitebread and Sorensen (1980) and Wallace (1977) revealed a compositionally variable intrusive suite that includes quartz monzonite and lesser amounts of diorite, gabbro, and aplitic and diabase dikes. The quartz monzonite yielded a 30.2 ± 2.5 Ma K/Ar biotite age (J. Obradovich, as cited in Whitebread and Sorensen, 1980). Zircon U-Pb dating by sensitive high-resolution ion microprobe (SHRIMP) of the diorite and quartz monzonite (this study) yielded 33.0 ± 0.3 Ma and 31.4 ± 0.4 Ma crystallization ages for the diorite and quartz monzonite phases of the pluton[1] (see GSA Data Repository) Oligocene plutons (ca. 28–24 Ma) and genetically related rhyolite ash flows are also present ~60 km southwest of Granite Mountain in the Stillwater Range and Clan Alpine Mountains (Riehle et al., 1972; John, 1995) (Fig. 1).

Ash-Flow Tuff (Taf)

The oldest Tertiary stratified rocks in the study area are rhyolitic ash-flow tuffs exposed in the southern Sou Hills (Figs. 2 and 3). Previously mapped and described by Nosker (1981), these tuffs unconformably overlie carbonate rocks of the Jurassic Winnemucca Formation (Fig. 3; Nosker, 1981). The ash-flow tuff in the Sou Hills is similar in composition to many tuffs erupted during the middle Tertiary "ignimbrite flare-up" ca. 35–20 Ma (e.g., Armstrong et al., 1969; Best et al., 1993). More locally, potentially correlative rhyolite ignimbrites in the Tobin Range (Fig. 1) span an age range of 33–25 Ma (Gonsior, 2006).

Older Basalt Flows (Tbo)

Rhyolite ash-flow tuffs are overlain by dark gray, porphyritic, vesicular basalt flows that are locally brecciated and oxidized to a reddish color (Fig. 3A). Basalt flows were deposited on top of the ash-flow tuff (Taf) and are also interbedded with the base of the overlying tuffaceous sedimentary unit (Tts) in the southwestern Sou Hills, suggesting that initial basin deposition was concomitant with basaltic magmatism. The source area and precise age of these basalts are not known. However, their stratigraphic position above the Oligocene ash-flow tuffs and overlying 17–15 Ma basalt flows (Tba) provide general late Oligocene to middle Miocene age constraints.

Tuffaceous Sedimentary Rocks (Tts)

Tuffaceous sedimentary rocks (Oligocene–Miocene[?]) overlie pre-Cenozoic basement in the East Range at McKinney Pass (Fig. 2), where they are poorly exposed and consist of white tuffaceous siltstone and sandstone with interbedded lenses of pebble conglomerate. As much as 700 m of tuffaceous siltstone overlies pre-Tertiary basement to the south along the eastern flank of the Stillwater Range. Variations in thickness and the map pattern of contacts suggest some local relief at the time of deposition. The lithology of this unit is more variable in the Sou Hills, where it is subdivided into two members (Fig. 3A). The lower member (Tts_l) consists of interbedded gray to beige volcaniclastic sandstone, pebble conglomerate, and well-lithified tuffaceous siltstone. The upper member (Tts_u) is characterized by interbedded, poorly consolidated tuffaceous and calcareous siltstone, pebble conglomerate, volcanic ash, and lacustrine diatomite.

Bimodal Volcanism: Olivine Basalt (Tba) and Rhyolite (Tr)

Sedimentary strata, tuffs, and pre-Cenozoic basement are all unconformably overlain by dark gray, vesicular olivine basalt flows (Tba) that range from 3 to 6 m thick in the Sou Hills to ~130 m thick in the East Range (Figs. 2 and 3). Small basaltic dikes and plugs are associated with these flows.

Published whole rock ages from these basalts in the East Range area show a range in ages from ca. 17–13 Ma (Nosker, 1981; Gonsior, 2006) (Fig. 3). The olivine basalts in the Sou Hills (Figs. 2 and 3) have K/Ar whole rock ages of 17.5 ± 0.9 Ma and 15.0 ± 0.7 Ma (Nosker, 1981). Gonsior (2006) obtained a $^{40}Ar/^{39}Ar$ whole rock age of 14.10 ± 0.12 Ma from basalt flows on the east side of the Tobin Range (Fig. 1) that overlie variably tilted Tertiary andesite flows, ash-flow tuffs, and sedimentary rocks similar to those exposed in the Sou Hills. Petrographically similar and younger olivine basalt at Table Mountain in the northern Stillwater Range (Fig. 1) unconformably overlies Tertiary sedimentary rocks and pre-Cenozoic basement (Speed, 1976). The youngest age from this unit, reported from the uppermost basalt flow that caps the northern Stillwater Range (Fig. 1), is 13.5 ± 0.5 Ma (Nosker, 1981).

[1]GSA Data Repository Item 2008066, Part 1—SHRIMP U-Pb Analytical Data (text, table and graphics), Part 2—Apatite fission track analytical data (text and graphics), and Part 3—Apatite (U-Th)/He analytical data (text, table), is available at www.geosociety.org/pubs/ft2008.htm. Requests may also be sent to editing@geosociety.org.

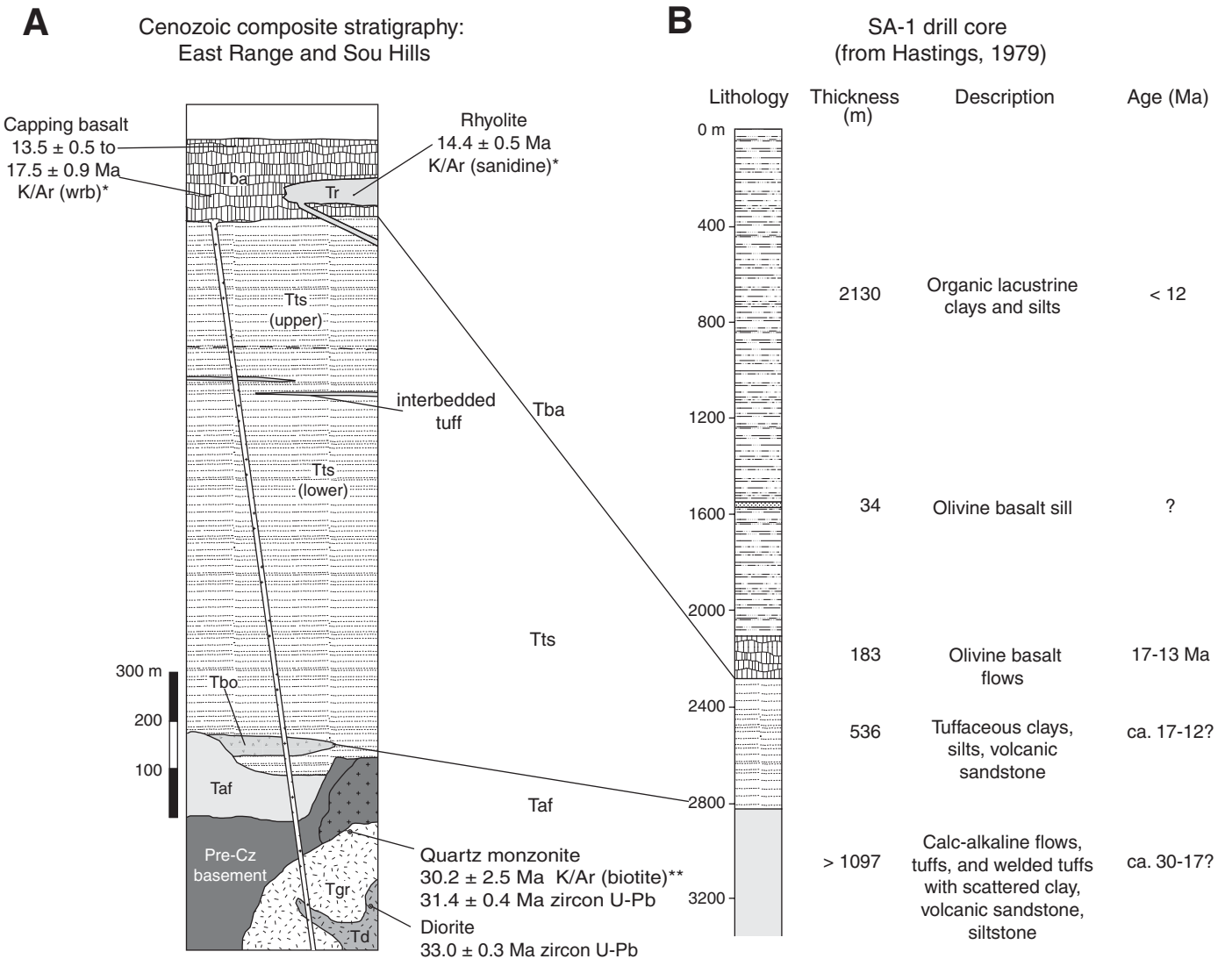

Figure 3. (A) Schematic composite stratigraphic section of Tertiary units in the East Range and Sou Hills. Previously published K/Ar ages and zircon U-Pb ages are shown. Asterisk (*) denotes ages obtained by Nosker (1981), and double asterisk (**) indicates age referenced in Whitebread and Sorensen (1980). (B) Schematic drill core (Standard-Amoco S.P. Land Co. no. 1) from the northern Carson Sink (Fig. 1), showing lithology, unit descriptions, and correlation with outcrop exposures in the Sou Hills (this study). Drill core log and ages simplified from Hastings (1979). Cz—Cenozoic; wrb—whole rock basalt; Taf—ash-flow tuff. See Figure 2 for other abbreviations.

Tertiary rhyolite flows and plugs (Tr) overlie and intrude, respectively, Oligocene–Miocene sedimentary rocks in the northern Sou Hills and the East Range at McKinney Pass (Figs. 2 and 3). Nosker (1981) obtained a 14.4 ± 0.5 Ma K/Ar age from this rhyolite dome. Additional geochronology and geochemistry of the olivine basalts in the Sou Hills area would greatly improve the temporal resolution of bimodal volcanic activity, particularly in relation to the timing of normal faulting.

Correlation with Subsurface Stratigraphic Data

The Cenozoic stratigraphic sequence of the Sou Hills and East Range can be correlated with similar lithologic units that are now buried in nearby basins (Fig. 3). A borehole in northern Carson Sink (Hastings, 1979) (Fig. 1) records a continuous 3353-m-thick Tertiary section consisting of an older volcanic member of calc-alkaline flows and sedimentary rocks (i.e., Taf), overlain by poorly consolidated tuffaceous sedimentary rocks (i.e., Tts), and capped by olivine basalt and basaltic andesite flows (i.e., Tba) (Fig. 3B). On the basis of similar composition and thickness, we correlate this section with stratified units exposed in the Sou Hills (Fig. 3) and infer that it has been displaced by range-bounding faults in the Stillwater Range (Fig. 2). Given the 45 km distance between the drill hole and outcrop in the Stillwater Range and Sou Hills (Fig. 1), this correlation is made with caution, and we acknowledge the likely existence of paleotopography during deposition. The "capping basalt" (Tba) that crops out in the Stillwater East and Humboldt Ranges probably offers the most reliable correlation, and thus it is used in the deformational reconstructions given below.

Cenozoic Structure of the Sou Hills

Previous workers have suggested that Cenozoic rocks in the Sou Hills were uplifted and tilted in a zone of deformation between two overlapping, oppositely dipping normal

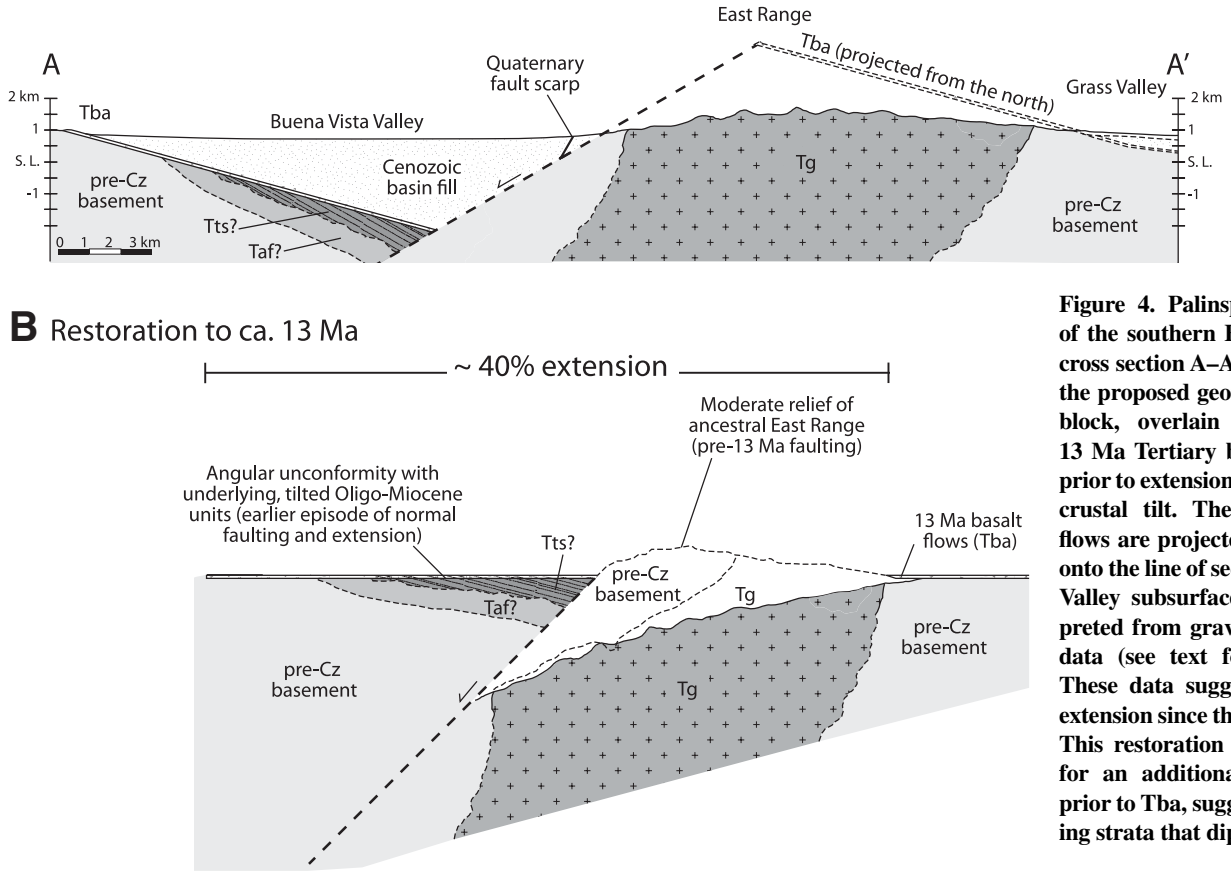

Figure 4. Palinspastic restoration of the southern East Range, along cross section A–A′ (Fig. 2), restores the proposed geometry of the fault block, overlain by the capping 13 Ma Tertiary basalt flows (Tba) prior to extension and 15° eastward crustal tilt. The youngest basalt flows are projected from the south onto the line of section. Buena Vista Valley subsurface geometry interpreted from gravity and drill core data (see text for more details). These data suggest ~40% crustal extension since the eruption of Tba. This restoration does not account for an additional ~15° of tilting prior to Tba, suggested by underlying strata that dip 30°–40° east.

fault systems: the west-dipping Tobin Range Fault and the east-dipping Dixie Valley Fault (Fig. 1) (Stewart 1980; Faulds and Varga, 1998). In the southern Sou Hills, basalt flows (Tbo) and Oligocene(?) fluvial-lacustrine sedimentary rocks overlie a 30–35 Ma(?) ash-flow tuff and dip ~30° SE (Fig. 2). In the central Sou Hills, dips in these units change to predominantly north (25°–35°), indicating broad rotation and folding of the section (Fosdick, 2006). This geometry is interpreted as extension-related folding in the zone of overlap between two oppositely dipping normal faults, similar to systems studied elsewhere in the Basin and Range (e.g., Varga et al., 2004). On the eastern edge of the Sou Hills the southern extent of the west-dipping Tobin Range Fault cuts Tertiary sedimentary rocks that dip ~30°–45° SE (Fig. 2). Historic rupture of this segment of the fault indicates that the Sou Hills are still actively deforming (Wallace, 1984; Fonseca, 1988).

Younger (17–13 Ma) olivine basalt flows (Tba) unconformably overlie the Oligocene sedimentary rocks and ash-flow tuff and dip 12°–16° E (Fig. 2). The angular unconformity beneath the olivine basalt and the underlying units indicates that some tilting, folding, and warping of the basinal deposits occurred after ca. 30 Ma(?) and before the eruption of the olivine basalt flows at 17–13 Ma (Fig. 4A). The olivine basalts were subsequently truncated and tilted during displacement along the Sou Hills Fault after ca. 13 Ma.

Cenozoic Structure of the Southern East Range

Structural relations inferred from geologic mapping of east-dipping Tertiary strata in the southern East Range indicate that tilting took place in two phases. The first event is documented by Oligocene tuffaceous sedimentary rocks that dip 30°–45° E (Fig. 2). These units are unconformably overlain by 17–13 Ma olivine basalt flows that dip ~15°–20° E (Figs. 2 and 4A), suggesting that 10°–30° tilting occurred before the eruption of 17–13 Ma basalts. About 5 km north of Granite Mountain, correlative olivine basalts dip uniformly ~20° E and directly overlie pre-Cenozoic basement (Figs. 2 and 4A). These relationships suggest that there may be a total of at least 30° (and locally up to 45°) of eastward tilt of the East Range, about half of which occurred prior to the eruption of an olivine basalt sequence (>17–13 Ma).

Subsurface data from Buena Vista Valley (Figs. 2 and 5) offer more insight into the geometry and structure of the poorly exposed fault system bounding the East Range to the west. Gravity data indicate ~2.5 km of basin fill in Buena Vista Valley; the basin deepens southward and contains ~4 km of fill in Carson Sink (Erwin, 1974; Hastings, 1979). This valley and Dixie Valley (Fig. 1) are two of the deepest basins in the northern Basin and Range (Catchings and Mooney, 1991) consistent with significant amounts of slip on bounding faults.

Tertiary strata west of McKinney Pass (Fig. 2) dip ~20°–30° east, and we infer that the East Range footwall block in the vicinity of Kyle Hot Spring is tilted a similar amount (Fig. 2). If this is correct, the fault would now dip ~30°–40° (assuming an initial dip of

60° W). A moderately dipping fault is consistent with the rather low ~3–4 mgal/km gravity gradient across Buena Vista Valley and the East Range, indicated by the gravity profile along section B–B′ in Figure 5. In contrast, much steeper gradients may result from high-angle normal faults, such as the ~9 mgal/km gradient across the fault bounding the Stillwater Range in Dixie Valley, which has been shown in seismic data to dip ~50° (Okaya and Thompson, 1985) and which may shallow at depth (Abbott et al., 2001). These gradients yield minimum estimates of dip; alternatively, large-scale landsliding and interbedded alluvial fans and playa sediments in this tectonically active setting could effectively lower the gravity gradient.

Hot springs and scarps in Quaternary alluvial fans along the western side of the East Range indicate high heat flow and recent fault activity. Detailed gravity surveys at Kyle Hot Spring (Fig. 2) indicate that a Quaternary high-angle fault system is responsible for localizing the spring (Goldstein and Paulsson, 1978). These faults are interpreted to accommodate the most recent extension by normal faulting, whereas large-magnitude extension that resulted in tilted Oligocene–Miocene units in the East Range is inferred to have taken place on an older, more shallowly dipping normal fault that has been rotated during uplift and block rotation (Fig. 2) (Fosdick, 2006).

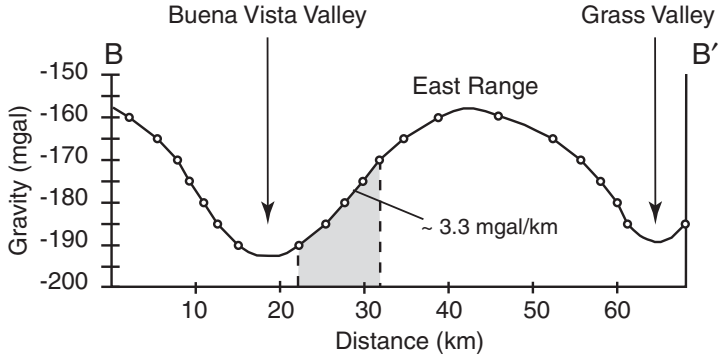

Figure 5. Bouguer gravity along section B–B′ in mgal (Fig. 2) across the East Range and parts of the Humboldt and Tobin Ranges (note 50% horizontal scale reduction from Fig. 2). These data along the western slope of the East Range indicate a nominal ~3.3 mgal/km gradient. This estimate is consistent with a moderately shallow fault contact between the basement and basin fill. Dashed contours indicate anomalies <–160 mgal.

Magnitude of Crustal Extension

Extensional strain in the East Range was partitioned into two major episodes of normal faulting. Oligocene–Miocene strata that predate the olivine basalt do not provide a continuous marker unit across the East Range; thus it is less clear how much extension occurred prior to 13–17 Ma. This older faulting was responsible for ~15° eastward tilting of Oligocene–Miocene sediments and underlying units in the Sou Hills and East Range (Fig. 4A). Based on ~15° dip of these tilted Oligocene–Miocene strata and an assumed 60° initial fault dip, we estimate that ~22% extension across the East Range occurred prior to eruption of the 17–13 Ma olivine basalts.

The second period of fault slip postdates the olivine basalt sequence (unit Tba, Fig. 2) and thus took place more recently than 17–13 Ma. To reconstruct this younger extension, east-dipping (15°) olivine basalts are extrapolated from the eastern flank of the Humboldt Range (Fig. 2) and beneath Buena Vista Valley to the East Range bounding fault (Fig. 4). The approximate subsurface geometry of this volcanic sequence is projected from the south (Fallon drill core) and is consistent with depth-to-basement gravity estimates for Buena Vista Valley (Erwin, 1974). Figure 4B illustrates the palinspastically restored geometry across the East Range (A–A′) at 17–13 Ma, equivalent to at least 40% extension (or ~11.5 km) since that time. This is a minimum strain estimate for the second faulting event, because the initial condition (Fig. 4A) includes the extensional strain from the first period of fault slip and tilting. Our nominal estimate of total strain is ~60%, indicating greater amounts of extension than values determined for the adjacent Tobin Range, where 40%–45% extension occurred during multiple episodes of faulting since the Oligocene (Gonsior, 2006) (Fig. 1).

APATITE (U-Th/He) AND FISSION TRACK THERMOCHRONOLOGY

Methodology

Apatite fission track and (U-Th)/He thermochronology have been used to determine the timing and magnitude of extension by normal faulting in many parts of the Basin and Range. Together, these methods can constrain the thermal history of a footwall block in detail, and, by proxy, the timing of fault slip, tilting, and exhumation (e.g., Foster et al., 1991; Fitzgerald et al., 1991; Foster and John, 1998; Surpless et al., 2002; Armstrong et al., 2003; Stockli, 2005; Carter et al., 2006; Colgan et al., 2006b; Metcalf, 2006). To quantify the timing of faulting and extension in the southern East Range, we collected a detailed E-W transect of samples across Granite Mountain, perpendicular to the range-bounding fault (Fig. 6A). Multiple single-grain (U-Th)/He analyses were obtained from 18 samples, and fission-track analyses from 10 samples. Apatite fission track and (U-Th)/He analytical data are shown in Table 1. Complete analytical data and procedures are reported in Table DR2[1] (see GSA Data Repository).

The fission track method is based on the accumulation of linear damage trails in the crystal lattice formed by the spontaneous fission decay of ^{238}U. In apatite, these "tracks" form with initially uniform lengths (~16 μm) at a constant rate through geologic time. They are completely annealed, or erased, at temperatures above ~120 °C, and retained below ~60 °C (e.g., Gleadow et al., 1986; Green et al., 1989), a temperature range termed the *partial annealing zone* (PAZ). Track density and measured track length thus vary systematically according to the thermal history (time-temperature path) of a given sample.

The (U-Th)/He method relies on the accumulation of α particles produced during the decay of ^{238}U, ^{235}U, and ^{232}Th nuclei. In an apatite crystal, α particles (^{4}He nuclei) escape the crystal lattice by thermally activated diffusion at temperatures above ~85 °C and are retained at temperatures below ~40 °C (Zeitler et al., 1987; Farley, 2000, 2002). At temperatures between 40 and 85 °C, termed the *partial retention zone* (PRZ; Wolf et al., 1996), ^{4}He gas is partially retained in the crystal lattice. ^{4}He is essentially immobile at temperatures below ~40 °C (Farley, 2000, 2002). For apatite crystals that cool relatively quickly (~10 °C/m.y.), the (U-Th)/He system is considered to have a nominal closure temperature (T_c) of ~70 °C (Wolf et al., 1996; Farley, 2002). The time-temperature path of an individual sample can be further constrained using computer models that solve for thermal history that best fits a given set of fission track grain ages, track lengths, and (U-Th)/He single grain ages (e.g., Ketcham 2005). Complete

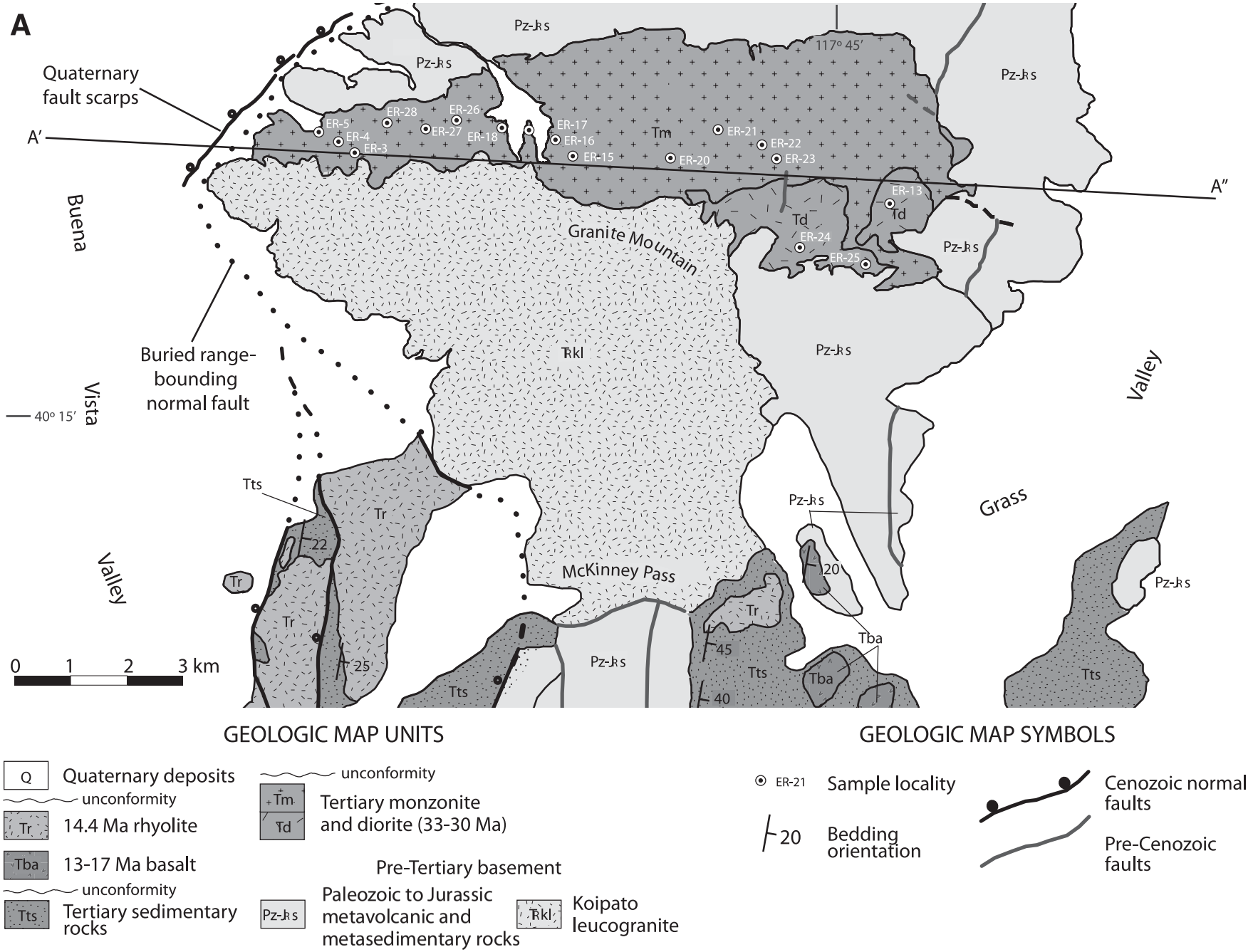

Figure 6. (A) Geologic map of the fault block through Granite Mountain, showing location of the thermochronologic sample transect (A′–A″). (*Continued on following page.*)

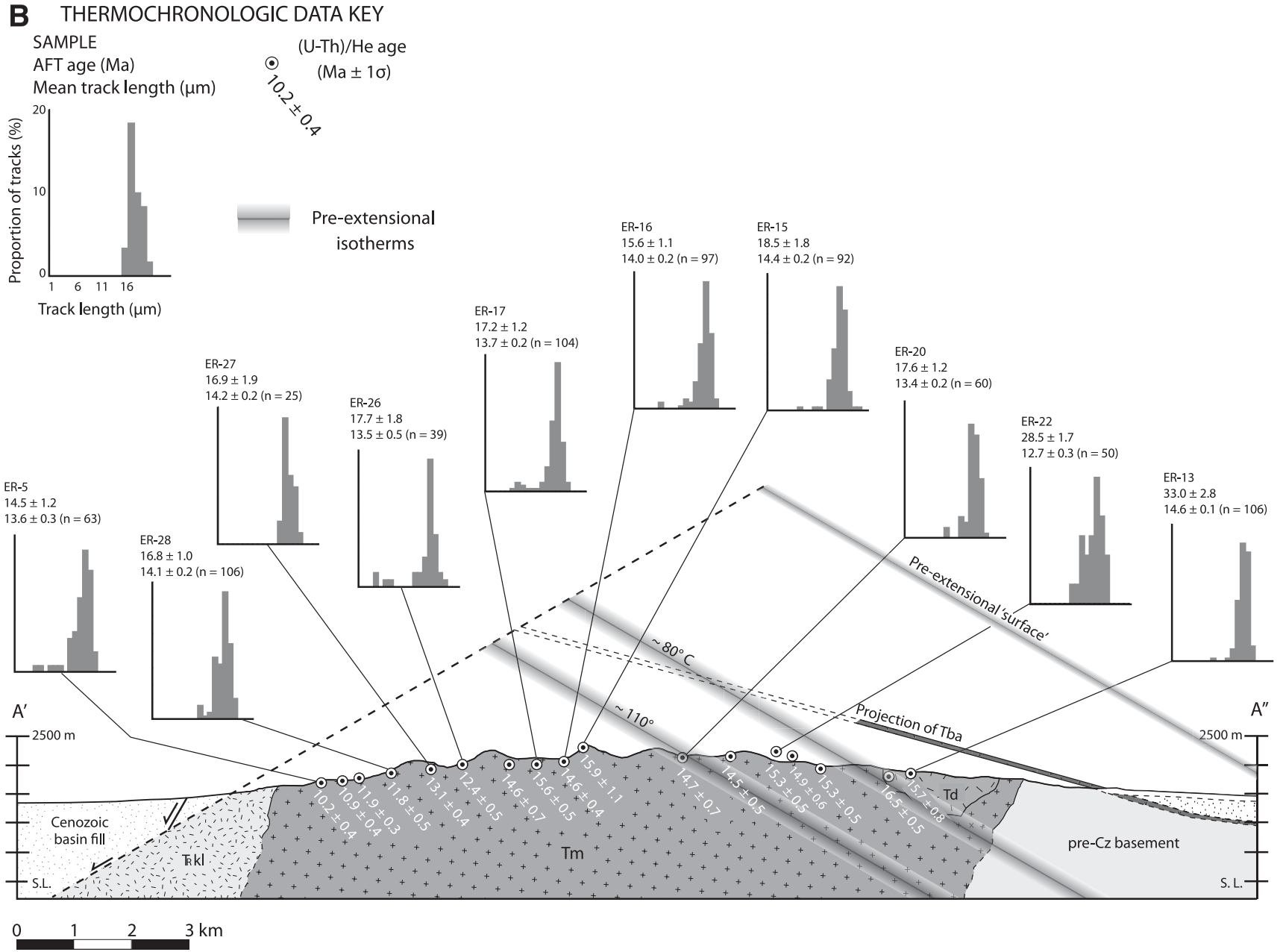

Figure 6. (*continued*) (B) Structural and thermal transect (A′–A″) of Granite Mountain, showing thermochronologic results and the preextensional thermal structure. Apatite fission track ages (in Ma) are shown above track length histograms, and apatite (U-Th)/He ages are displayed adjacent to the sample localities. Thick gray lines indicate preextensional isotherms based on inflection points in the thermochronologic data (see text for discussion on constructing paleodepths). The basal Tertiary unconformity beneath Tba is projected from the south. AFT—apatite fission track.

TABLE 1. APATITE (U-Th)/He AND FISSION TRACK DATA FROM GRANITE MOUNTAIN, EAST RANGE, NEVADA

Sample number	Latitude (°N)	Longitude (°W)	Elevation (m)	Paleodepth (km)†	FT age (Ma ± 1σ)‡	Mean track length (mm ± 1σ)	Weighted He age (Ma ± 1σ)
East Range (A′–A″)							
ER-5	40.2949	–117.8612	1549	8.24	14.5 ± 1.2	13.64 ± 0.13	10.1 ± 0.4
ER-4	40.2934	–117.8571	1592	8.03			10.9 ± 0.4
ER-3	40.2917	–117.8537	1640	7.85			11.9 ± 0.3
ER-28	40.2965	–117.8469	1725	7.49	16.8 ± 1.0	14.06 ± 0.15	11.8 ± 0.5
ER-27	40.2956	–117.8380	1777	7.10	16.9 ± 1.1	14.23 ± 0.33	13.1 ± 0.4
ER-26	40.2970	–117.8325	1868	6.75	17.7 ± 1.8	13.5 ± 0.55	12.4 ± 0.5
ER-18	40.2958	–117.8230	1871	6.35			14.6 ± 0.7
ER-17	40.2954	–117.8174	1877	6.11	17.2 ± 1.2	13.66 ± 0.22	15.6 ± 0.5
ER-16	40.2939	–117.8118	1923	5.83	15.6 ± 1.1	13.96 ± 0.18	14.6 ± 0.4
ER-15	40.2914	–117.8082	2168	5.45	18.5 ± 1.8	14.42 ± 0.16	15.9 ± 1.1
ER-20	40.2912	–117.7878	2005	4.75	17.6 ± 1.2	13.94 ± 0.19	14.7 ± 0.7
ER-21	40.2958	–117.7780	2027	4.31			14.5 ± 0.5
ER-22	40.2935	–117.7687	2089	3.85	28.5 ± 1.7	12.69 ± 0.27	15.3 ± 0.5
ER-23	40.2913	–117.7656	2023	3.77			14.9 ± 0.6
ER-24	40.2775	–117.7606	1816	3.72			15.3 ± 0.5
ER-25	40.2746	–117.7469	1648	3.25			16.5 ± 0.5
ER-13	40.2842	–117.7420	1737	3.18	33.0 ± 2.8	14.55 ± 0.11	15.7 ± 0.8

†Preextensional paleodepth is measured as distance beneath the basal Tertiary tuffaceous sedimentary rocks in the East Range that dip 30° east and rest unconformably on Paleozoic and Mesozoic footwall rocks.
‡FT age is the fission track central age of Galbraith and Laslett (1993).

analytical data and procedures are reported in Table DR3 (see footnote 1).

Preextensional Depth of Thermochronology Samples

In studies that relate thermochronologic data to large-scale faulting, it is useful to define a paleohorizontal reference datum in order to estimate the depth of samples in the crust prior to exhumation (e.g., Fitzgerald et al., 1991; Foster and John, 1998; Miller et al., 1999). In much of the Basin and Range, the profound angular unconformity at the base of the Tertiary (the "basal Tertiary unconformity") is ideal for this purpose. However, at Granite Mountain (Fig. 6) the basal Tertiary unconformity is concealed by Quaternary deposits. Therefore, we estimate preextensional paleodepths across the East Range (Fig. 6B) by combining depth estimates from thermochronologic data with estimated tilt from structural relationships in nearby areas. The southern East Range has undergone an average 30° of total cumulative eastward footwall tilt, judging by preextensional Oligocene–Miocene volcanic and sedimentary rocks in nearby exposures (Fig. 2). We thus assume that all preextensional horizontal features have been tilted 30° and calculate paleodepths below the inferred preextensional land surface by evaluating the thermal parameters necessary to satisfy the apatite fission track (AFT) and apatite (U-Th)/He (AHe) data. Recent modeling studies have shown the impact of upward advection of isotherms during rapid uplift and erosion (e.g., Bertotti and ter Voorde, 1994; Ehlers et al., 2003; Armstrong et al., 2003). These processes, in addition to coeval magmatism during exhumation, are understood to cause higher geothermal gradients and reduced estimates of structural depth. In this paper we do not provide a detailed thermal model to account for these processes; thus the thermochronologic constraints described here impart a first-order approximation of the magnitude of structural depth and exhumation.

The structurally highest fission-track age inferred to be fully reset prior to faulting (sample ER-20, Fig. 6B) is assumed to have resided at a preextensional paleodepth approximating the ~110 °C isotherm. All AFT samples below this depth have long track lengths and reset ages (Fig. 6B), consistent with temperatures >110 °C (until cooling). In contrast, samples at crustal levels above sample ER-20 are interpreted as partially reset, consistent with long residence time *within* the AFT PAZ (110–60 °C) (Fig. 6B).

The depth of the preextensional AHe PRZ is similarly inferred by AHe and AFT data superimposed on the tilted fault block (Fig. 6B). Sample ER-13 exhibits an AFT age of 33.0 ± 2.8 Ma and long track lengths but yielded a significantly younger AHe age at ca. 15 Ma, consistent with temperatures between ~80 and 60 °C prior to 15 Ma. Thus, we infer the 80° isotherm to be structurally near to sample ER-13 and likely above the underlying, reset AHe samples (Fig. 6B). Samples below this depth are inferred to have had zero AHe ages before the onset of rapid cooling at ca. 15 Ma.

The 110 and 80 °C isotherms, projected across the range with a ~30° east tilt, provide the basis for preextensional paleodepths through the East Range (Fig. 7) and are used in the following discussion of thermochronologic data. Paleodepth is measured beneath the projected 10 °C isotherm, restored to horizontal at ca. 20 Ma. Although the depth and shape (i.e., flat versus curved) of the 10 °C isotherm—and thus the "paleodepth" of samples relative to the Miocene land surface—are necessarily an approximation, and the structural positions of adjacent samples *relative to each other* are well constrained and depend only on the tilt of the footwall block. Assuming a 30° tilt of the East Range, the samples discussed below span ~5.5 km of structural relief.

Apatite Fission Track Data and Results

Apatite fission track (AFT) results (Table 1) show a systematic decrease in age with increasing paleodepth from east to west toward the range-bounding fault (Figs. 6 and 7). AFT ages decrease from 33 to 15 Ma and cluster at ca. 17 Ma at inferred paleodepths >~4.8 km (Fig. 7). The oldest, and shallowest (~3.2 km paleodepth), AFT age (ER-3; 33.0 ± 2.8 Ma) is within error of the 33.0 ± 0.3 Ma crystallization age of the diorite pluton, suggesting rapid post-intrusion cooling of the pluton to temperatures <60 °C at 33 Ma. From ~3.0–4.8 km paleodepth (Fig. 7), AFT ages become progressively younger and exhibit shorter mean track lengths (Fig. 6). For example, sample ER-22 has a 12.69 ± 0.27 μm mean track length and a 28 Ma age that we interpret to indicate partial resetting within the PAZ prior to unroofing.

The 12 samples structurally below sample ER-22, between ~4.8–7.5 km paleodepth, have AFT ages that average ca. 17 Ma (Fig. 7) and exhibit relatively long track lengths (e.g., ER-15, Fig. 6B). The structurally deepest sample (ER-5; ~8.2 km paleodepth) exhibits a shorter mean track length (13.64 ± 0.3 μm) and a 14.5 ± 1.2 Ma AFT age (Figs. 6 and 7); this sample is notably younger than AFT ages reported from structurally higher samples.

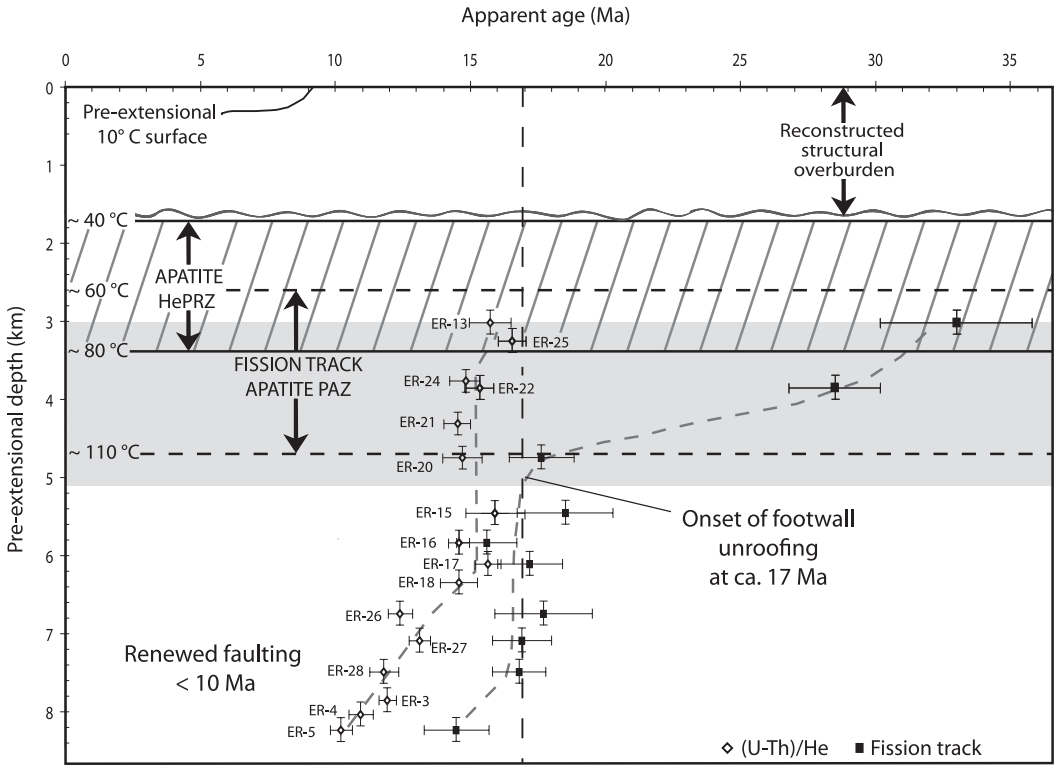

Figure 7. Apatite fission track (AFT) and (U-Th)/He ages (±1σ) plotted against reconstructed paleodepth based on Tertiary sedimentary and volcanic rocks that dip 30° E and were deposited unconformably on nearby pre-Cenozoic basement. Thick gray lines are preextensional isotherms based on inflection points in the thermochronology. The AFT partial annealing zone (PAZ, gray rectangle) and the helium partial retention zone (HePRZ, hachured rectangle) are based on these isotherms and a nominal ~23 °C/km Miocene geothermal gradient. Refer to Figure 6 for track lengths and sample locations.

Apatite (U-Th)/He Data and Results

Apatite (U-Th)/He (AHe) results from Granite Mountain show a systematic E-W decrease in age from ca. 16–10 Ma toward the range-bounding fault (Fig. 6). We interpret all AHe ages to have been partially or completely reset prior to exhumation (i.e., all sample sites resided within or below the AHe PRZ at 16 Ma). Shallower than ~3 km paleodepth, samples display slightly older AHe ages with significant replicate variability (Table 1); these data may represent only partial resetting and helium loss during residence at the basal part of the AHe PRZ prior to the onset of cooling. From ~3.6–6.4 km paleodepth, AHe ages cluster at ca. 15 Ma (Fig. 7). These samples overlap with the depth range in which reset AFT cooling ages cluster at ca. 17 Ma. From 6.1 to 8.2 km paleodepth, AHe ages show a systematic decrease in age from ca. 15–10 Ma (Figs. 6 and 7). Sample ER-5 yields the youngest AHe age (10.21 ± 0.4 Ma) and also the youngest AFT age (14.5 ± 1.2 Ma) (Fig. 8).

Thermochronologic Data Modeling

Inverse modeling of AHe and AFT data from the East Range transect places additional constraints on the time-temperature history of the footwall block. AFT and AHe data were modeled using the HeFTy® program of Ketcham (2005). Together, these systems are sensitive to the thermal history of a sample between ~120 and 40 °C. Modeled time-temperature paths from four representative samples are shown in Figure 8.

Cooling of the structurally shallowest samples through most of the AFT PAZ in the East Range appears to significantly predate faulting. Modeling of sample ER-22 (Fig. 8A) suggests that the top (upper 4 km?) of the 31 Ma pluton underwent rapid post-intrusion cooling, followed by prolonged residence within the upper part of the PAZ until roughly 15 Ma. This is consistent with the slightly shortened mean track length of 12.67 ± 0.27 μm in this sample (Fig. 6). Samples beneath the AFT PAZ and HePRZ (3.5–6.4 km paleodepth, Fig. 7) constrain the timing of rapid cooling. Modeling of sample ER15 (Fig. 8B) indicates rapid exhumation through both the apatite PAZ and HePRZ at 17–16 Ma, presumably followed by slower cooling from ~40 °C to present-day surface temperature, although the data are not sensitive to temperatures this low (Fig. 8B). We interpret these data, and similar cooling histories from nearby samples, to represent rapid cooling during exhumation and fault slip at ca. 17–15 Ma.

Model results from sample ER-26 (~8 km paleodepth) are inferred to reflect crust exhumed by faulting that is more recent than ca. 10 Ma (Fig. 7). Sample ER-26 cooled to 80–60 °C from 17 to 15 Ma but remained above ~40 °C during this time interval (Fig. 8C). The modeled thermal history is consistent with this sample having resided in the AHe PRZ until renewed cooling began after ca. 10 Ma (Fig. 8C). Similarly, results from sample ER-5, the deepest sample (8.2 km), suggest significant cooling after ca. 10 Ma (Fig. 8D), with a poorly constrained early history that likely corresponds to the 17–16 Ma event documented in shallower samples. Conspicuous short track lengths in sample ER-5 are interpreted to be the result of partial annealing during the 17–15 Ma interval, prior to renewed faulting more recently than 10 Ma.

Thermochronologic Data Interpretations

Apatite (U-Th)/He and fission track data presented here document rapid middle to late Miocene exhumation and cooling of the East Range footwall block. Results from AFT and AHe dating and inverse modeling of these data are interpreted to record rapid slip along normal faults at 17–15 Ma (Fig. 6), leading to exhumation of nearly 3.5 km of upper crust to within 2 km of the Earth's surface (Fig. 7). AHe cooling ages provide an additional timing constraint and show that the upper ~2.8 km of this crustal section was exhumed to temperatures below 40 °C over approximately the same time

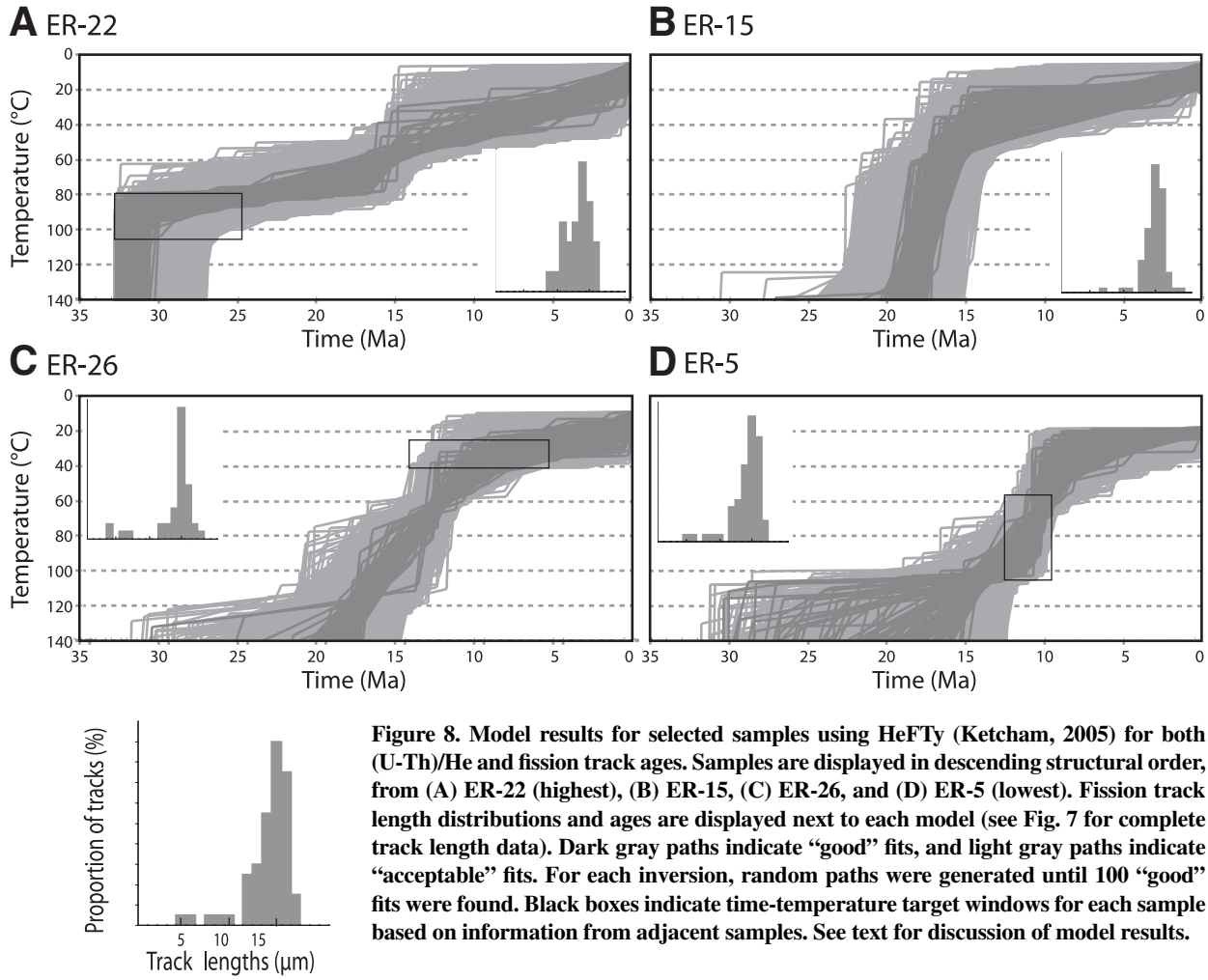

Figure 8. Model results for selected samples using HeFTy (Ketcham, 2005) for both (U-Th)/He and fission track ages. Samples are displayed in descending structural order, from (A) ER-22 (highest), (B) ER-15, (C) ER-26, and (D) ER-5 (lowest). Fission track length distributions and ages are displayed next to each model (see Fig. 7 for complete track length data). Dark gray paths indicate "good" fits, and light gray paths indicate "acceptable" fits. For each inversion, random paths were generated until 100 "good" fits were found. Black boxes indicate time-temperature target windows for each sample based on information from adjacent samples. See text for discussion of model results.

interval, ca. 15.2 ± 0.2 (1σ) (weighted mean of 12 invariant AHe ages) (Fig. 7).

Distinctly younger AHe cooling ages from samples adjacent to the range-bounding fault (within 3 km) (Fig. 6) are interpreted to record renewed exhumation by fault slip more recently than 10 Ma (Fig. 6). We interpret this progressive westward age reduction seen in the footwall block to reflect partial resetting of the structurally deepest samples following rapid 17–15 Ma cooling. For example, the thermal history of sample ER-5 is consistent with partial resetting in a younger PRZ established as the first faulting event waned, analogous to the situation documented in the Wassuk Range and White Mountains by Stockli et al. (2002, 2003), where Miocene faulting was followed by renewed Pliocene activity. The youngest sample constrains the maximum timing for the onset of reactivated faulting (10.21 ± 0.4 Ma). In addition, the youngest AFT age (14.5 ± 0.4 Ma) within this depth range is significantly younger than AFT ages from shallower paleodepths and has significantly shorter tracks (Fig. 6B), consistent with partial resetting. We infer that this second episode of faulting exhumed an additional ~1 km of crust through the AHe PRZ (>1.5 km depth), resulting in nearly 5 km of tilted upper crust now exposed across Granite Mountain (Fig. 7). An alternative interpretation is that these younger ages record a single, more protracted cooling (and thus faulting) event with a somewhat lesser total magnitude of vertical exhumation (<0.5 km).

Reconstructed temperature-depth estimates imply a nominal preextensional geothermal gradient of ~23 °C/km for the upper crust prior to faulting, generally consistent with other values of Miocene geothermal gradients in the central Basin and Range (e.g., Stockli et al., 2002; Ehlers and Farley, 2003). However, the uncertainty of this value is substantial owing to the approximations of both paleoisotherms and crustal tilt. Moreover, advection of shallow isotherms during rapid uplift and erosion and concurrent magmatism probably elevated the geothermal gradient (e.g., Ehlers and Farley, 2003; Ehlers, 2005), and thermal modeling of these processes is necessary to provide a better picture of the thermal evolution of the East Range footwall block (e.g., Ehlers et al., 2003).

DISCUSSION AND CONCLUSIONS

Two-Stage Faulting History

Thermochronologic data and structural relationships within Tertiary strata are consistent with a two-phase history of Miocene extension in the East Range and Sou Hills (Fig. 7). The oldest sedimentary and volcanic rocks in the area record cumulative tilting of ~30°–45°E (Figs. 4 and 9), whereas younger basalt flows indicate only a 15°–20°E tilt since 17–13 Ma (Figs. 4 and 6). Cumulative fault slip during these two episodes resulted in ~60% extensional strain across the East Range.

Thermochronologic data indicate rapid exhumation of ~6.4 km of crustal section (~4.8 km

documented by these data and an additional ~1.6 km of inferred structural overburden) at 17–15 Ma (Figs. 6 and 7). Younger AHe and AFT ages near the range-front fault are interpreted to record renewed faulting after 10 Ma that exhumed an additional >1 km of crust to within ~1.5 km of the surface (Fig. 7). Eruption of the middle Miocene basalt flows (Fig. 2) overlaps in time with the 17–15 Ma phase of normal faulting, with the most significant and widespread activity centered ca. 14–13 Ma. Therefore we infer that volcanism began shortly after some exhumation and tilting had already taken place (accounting for the angular unconformity at the base of the basalt flows) and that some faulting and tilting occurred after volcanism had ceased (resulting in the present 15°–20° tilt of the basalt flows). It is unclear, however, if tilting of the basalt flows took place during the waning stages of the middle Miocene faulting documented by the thermochronologic data or if all or part of the observed 15°–20° of tilting took place during younger, post–10 Ma faulting.

A two-part extensional history of the East Range is outlined in Figure 9. Miocene (17–13 Ma) olivine basalt flows are extrapolated from outcrops east of McKinney Pass to cross section A–A′, resulting in the unconformity beneath these flows having cut down through isotherms constructed from AHe and AFT data (Fig. 6). We use this cross-cutting relationship to infer the approximate volume of rock eroded after 17–15 Ma fault slip, prior to the eruption of the youngest olivine basalt onto the eroded landscape (Fig. 9). The data do not resolve whether the two episodes of slip occurred along the same original fault, which rotated to progressively lower angles, or if the second phase of extension took place on a new, higher-angle fault. The simplest case is illustrated in Figure 9, where slip occurred on the same fault and accommodated up to a 30° tilt of Tertiary strata with a concomitant 30° rotation of the fault. In this interpretation, Quaternary fault scarps merge into this 30° fault (Figs. 4 and 9); alternatively, they may cut it at depth. A two-part exhumation and faulting history in the East Range is consistent with geologic relationships in the nearby Tobin Range to the east (Fig. 1), where extension began ca. 33 Ma and led to 5°–20° of structural tilt in at least two distinct phases. There, each phase of extension is inferred to have taken place along high-angle faults that cut and offset older faults, although the structures themselves are not well constrained (Gonsior, 2006; Gonsior and Dilles, 2008).

Tertiary Extension and Volcanism

Oligocene–early Miocene volcanism in the East Range Hills is part of the "ignimbrite flareup" that swept southward across central Nevada in the middle Tertiary (e.g., Armstrong and Ward, 1991) and is generally attributed to upwelling asthenosphere, possibly in the wake of a delaminating Farallon slab (e.g., Humphreys, 1995). The lack of an angular unconformity within the 33–20 Ma(?) volcanic and sedimentary rocks indicates that little, if any, deformation accompanied volcanism. This is consistent with several recent studies that document a relatively low-relief, tectonically quiescent Eocene to Oligocene landscape in western Nevada characterized by external westward drainage through east-trending paleovalleys (Gonsoir, 2006; John et al., 2008; Henry, 2008; Gonsior and Dilles, 2008). It is starkly at odds, however, with the rapid (strain rate $>10^{13}$), large magnitude (>100%) extension inferred to have taken place at 24.3 Ma in the southern Stillwater Range (Fig. 1) (Hudson et al., 2000). If significant Oligocene extension did take place in the southern Stillwater Range, then a profound structural transition zone must exist between there and the East Range.

Middle Miocene (17–13 Ma) basalts in the East Range and Sou Hills have not been precisely dated, but they broadly overlap, chemically and temporally, with 16.5–15.0 Ma basalts in the northern Nevada rift to the east (Zoback et al., 1994; John et. al., 2000). The angular unconformity between Miocene basalts and older volcanic rocks in the East Range and Sou Hills indicates that extension began prior to volcanism, and the 17–15 Ma exhumation documented by thermochronologic data means that volcanism took place during or immediately after faulting. More detailed mapping and precise dating of individual flows are necessary to work out the relative timing of extension (tilting) and basaltic volcanism, but it is clear that these processes are closely associated in space and time in the East Range. Middle Miocene basalts in the northern Nevada rift and northwestern Nevada are in turn part of the much larger Steens–Columbia River flood basalt province that extends into Oregon and Washington and represents the initial eruptions of the Yellowstone hotspot (e.g., Pierce and Morgan, 1992).

The Yellowstone hotspot has been inferred to have some causal link to Basin and Range extension (Anders et al., 1989; Parsons et al., 1994; Mueller et al., 1999), but the area of most voluminous flood basalt eruptions (Washington and Oregon) remains largely unextended, and the 16.5 Ma plume impingement point near the McDermitt Caldera in northwestern Nevada did not begin extending until ca. 12 Ma (Colgan et al., 2004, 2006a) (Fig. 1). Nevertheless, a large body of data now documents significant middle Miocene extension across the northern and central Basin and Range (e.g., McQuarrie and Wernicke, 2005, and references therein). Thus, although there appears to be a large-scale temporal association between hotspot magmatism and extension, the distribution of extensional faulting suggests the influence of more local variations in crustal structure or boundary conditions.

Timing of Regional Extension in the Northwestern Basin and Range

Middle Miocene (ca. 17–15 Ma) extension in the East Range–Sou Hills area was broadly coeval with well-documented extension across much of the Basin and Range Province (e.g., Dickinson, 2002; McQuarrie and Wernicke, 2005). During this period, deformation was generally focused into discrete zones of high strain separated by unextended crustal blocks. Extended domains were characterized by high strain rates; closely spaced, highly tilted fault blocks; and, locally, the development of metamorphic core complexes (e.g., Proffett, 1977; Fitzgerald et al., 1991; Faulds et al., 1995; Miller et al., 1999; Snow and Wernicke, 2000; Stockli, 2005; Carter et al., 2006). In west-central Nevada the East Range (this study) and the adjacent Tobin Range (Gonsior, 2006) constituted a middle Miocene extensional domain that was separated from the extended Shoshone–Toiyabe Range domain to the east (Colgan et al., 2008) by the intact Fish Creek Mountains block (Fig. 1). Areas to the west and southwest of the East Range also underwent significant extension at this time (Proffett, 1977; Surpless et al., 2002), but northwestern Nevada remained essentially undeformed until the late Miocene (Colgan et al., 2006a). The East Range was thus close to the northwestern margin of the middle Miocene Basin and Range, although the exact location and structural nature of this boundary is now obscured by younger faulting.

A second, distinctly younger period of faulting began in the East Range at or more recently than ca. 10 Ma, roughly coincident with the onset of faulting at 12 Ma in northwestern Nevada (Whitehill et al., 2004; Colgan et al., 2006a), along the western margin of the Basin and Range near Reno (Trexler et al., 2000; Henry and Perkins, 2001), and in the White Mountains (Stockli et al., 2003). Late Miocene (post-10–12 Ma) faulting has also been documented in the Toiyabe and Shoshone Ranges to the east (where it overprints strong middle Miocene extension), and the Cortez Range (where it does not) (Colgan et al., 2008). In contrast to earlier, middle Miocene extension, late Miocene and younger faulting took place

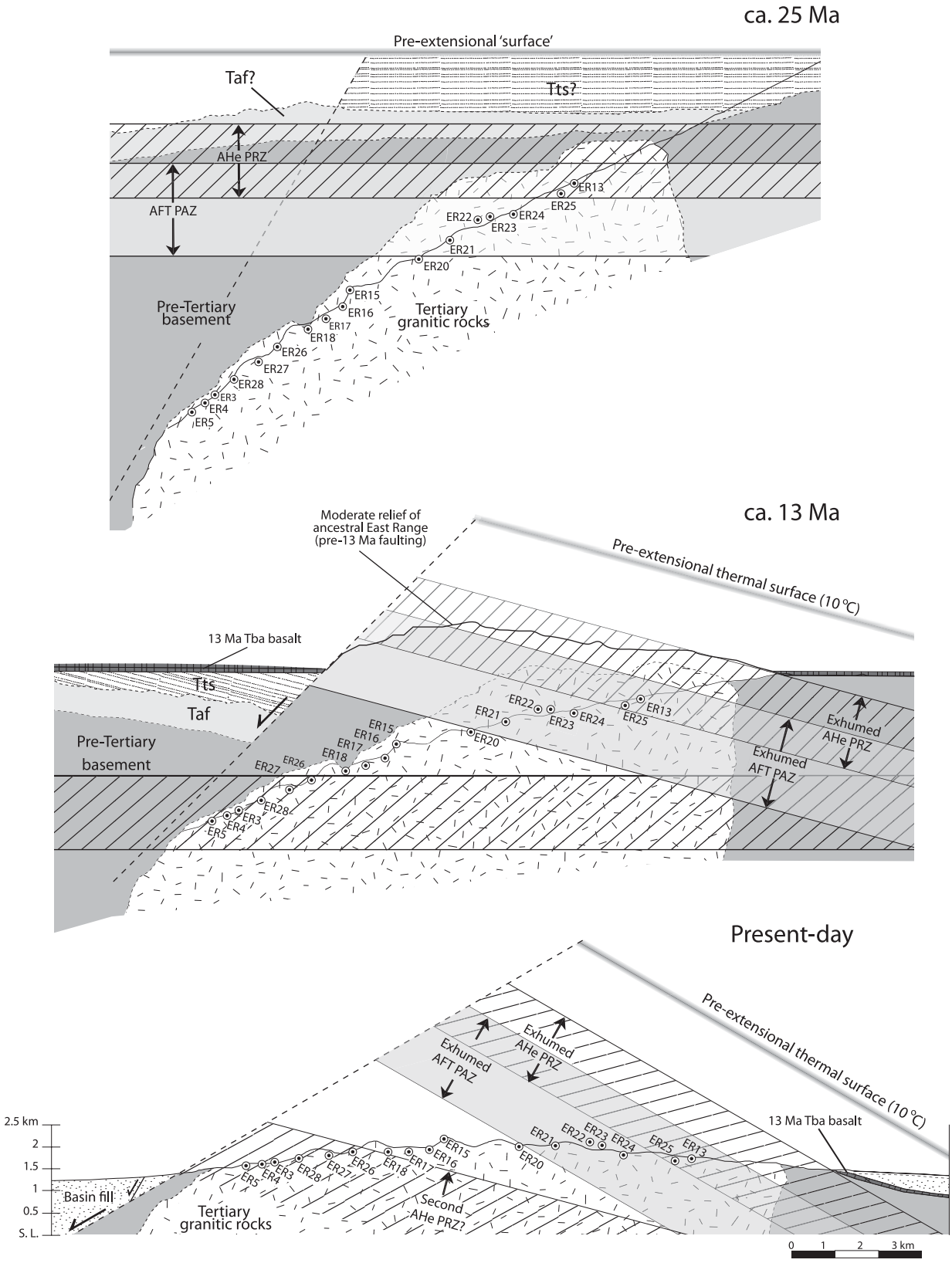

Figure 9. Two-stage structural and thermal reconstruction of extension of the southern East Range. Combined thermochronology and structural interpretation suggests a two-part history, in which rapid extension at 17–15 Ma exhumed part of the footwall, followed by subsequent normal faulting <10 Ma. AFT—apatite fission track; PAZ—partial annealing zone; PRZ—partial retention zone.

on widely spaced (20–30 km), high-angle faults that accommodated relatively small amounts of strain (<20%) but that affected a large area, overprinting older extensional domains (of both high and low strain) and creating the modern ranges in northern and western Nevada. It is unclear at present, however, if there was a significant time gap in western and central Nevada between rapid middle Miocene extension and the onset of late Miocene high-angle faulting.

Although younger (post-10–12 Ma) faulting affected previously unextended crust in western Nevada and thus can be said to represent westward "encroachment" of the Basin and Range (e.g., Surpless et al., 2002), it also clearly affected much of the previously extended Basin and Range to the east. Late Miocene and younger faulting thus appears to be a distinct, younger phase of extension characterized by a very different structural style rather than a simple westward migration of extension over time. Further complicating the late Miocene kinematic and temporal distribution of strain along the western Basin and Range is the northward propagation of the Walker Lane (Fig. 1). Dextral faulting in the Reno area, beginning ca. 9 Ma, may have diffused eastward and initiated and/or reactivated extension across a broader part of the northern Basin and Range (e.g., Faulds et al., 2005). Overall, the strong partitioning of middle Miocene deformation into extended and unextended domains may reflect a more profound influence of local heterogeneities in crustal structure or strength, whereas the more broadly distributed late Miocene extension may reflect the dominance of regional plate boundary processes that began in the late Miocene (e.g., McQuarrie and Wernicke, 2005).

ACKNOWLEDGMENTS

We wish to acknowledge Elizabeth Miller, Trevor Dumitru, and George Thompson for their insightful discussions, James Metcalf for assistance in the Noble Gas Laboratory at Stanford University, and Joe Wooden, Frank Mazdab, and Ariel Strickland for their help with U-Pb SHRIMP analyses. We also thank Thomas Carpenter, Randy Morris, Noah Morris, Karen Vasko, and Elizabeth Clark for assistance in the field. Derek Lerch and Carrie Whitehill provided helpful dialogue on Basin and Range geology. The scope and quality of this manuscript greatly benefited from the constructive and thoughtful reviews provided by James Faulds, Shari Kelley, and David Foster. Financial support for this study was provided by the Stanford University McGee Fund, GSA Student Research grant 8257-06, the Shell Foundation, and U.S. National Science Foundation grant EAR-0229854 to E.L. Miller.

REFERENCES CITED

Abbott, R.E., Louie, J.N., Caskey, S.J., Pullammanappallil, S., 2001, Geophysical confirmation of low-angle normal slip on the historically active Dixie Valley Fault, Nevada: Journal of Geophysical Research, v. 106, p. 4169–4181.

Anders, M.H., Geissman, J.W., Piety, L.A., and Sullivan, J.T., 1989, Parabolic distribution of circumeastern Snake River Plain seismicity and latest Quaternary faulting: Migratory pattern and association with the Yellowstone hotspot: Journal of Geophysical Research, v. 94, p. 1589–1621.

Armstrong, P.A., Ehlers, T.A., Chapman, D.S., Farley, K.A., and Kamp, P.J., 2003, Exhumation of the central Wasatch Mountains, Utah; 1, Patterns and timing of exhumation deduced from low-temperature thermochronology data: Journal of Geophysical Research, v. 108, p. 2172, doi: 10.1029/2001JB001708.

Armstrong, R.L., and Ward, P.L., 1991, Evolving geographic patterns of Cenozoic magmatism in the North American Cordillera: The temporal and spatial association of magmatism and metamorphic core complexes: Journal of Geophysical Research, v. 96, p. 13,201–13,224.

Armstrong, R.L., Ekren, E.B., McKee, E.H., and Noble, D.C., 1969, Space-time relations of Cenozoic silicic volcanism in the Great Basin of the western United States: American Journal of Science, v. 267, p. 478–490.

Bennett, R.A., Wernicke, B.P., Niemi, N.A., Friedrich, A.M., and Davis, J.L., 2003, Contemporary strain rates in the northern Basin and Range province from GPS data: Tectonics, v. 22, p. 1008–1039, doi: 10.1029/2001TC001355.

Bertotti, G., and ter Voorde, M., 1994, Thermal effects of normal faulting during rifted basin formation; 2, The Lugano–Val Grande normal fault and the role of preexisting thermal anomalies: Tectonophysics, v. 240, p. 145–157, doi: 10.1016/0040-1951(94)90269-0.

Best, M.G., Scott, R.B., Rowley, P.D., Swadley, W.C., Anderson, R.E., Gromme, C.S., Harding, A.E., Deino, A.L., Christiansen, E.H., Tingey, D.G., and Sullivan, K.R., 1993, Oligocene–Miocene caldera complexes, ash-flow sheets, and tectonism in the central and southeastern Great Basin, *in* Lahren, M., et al., eds., Crustal evolution of the Great Basin and the Sierra Nevada: Reno, University of Nevada, p. 285–311.

Burke, D.B., 1977, Geologic map of the southern Tobin Range, Pershing County, Nevada: U.S. Geological Survey Open-File Report OF 77-0141, scale 1:24,000, 1 sheet.

Carter, T.J., Kohn, B.P., Foster, D.A., Gleadow, A.J.W., Woodhead, J.D., 2006, Late-stage evolution of the Chemehuevi and Sacramento detachment faults from apatite (U-Th)/He thermochronometry; evidence for mid-Miocene accelerated slip: Geological Society of America Bulletin, v. 118, p. 689–709.

Caskey, S.J., Bell, J.W., Slemmons, D.B., and Ramelli, A.R., 2000, Historical surface faulting and paleoseismology of central Nevada seismic belt; Great Basin and Sierra Nevada: Boulder, Colorado, Geological Society of America Field Guide, v. 2, p. 23–44.

Catchings, R.D., and Mooney, W.D., 1991, Basin and Range crustal and upper mantle structure, northwest to central Nevada: Journal of Geophysical Research, v. 96, p. 6247–6267.

Colgan, J.P., Dumitru, T.A., and Miller, E.L., 2004, Diachroneity of Basin and Range faulting and Yellowstone hotspot volcanism in northwestern Nevada: Geology, v. 32, p. 121–124, doi: 10.1130/G20037.1.

Colgan, J.P., Dumitru, T.A., McWilliams, M.O., and Miller, E.L., 2006a, Timing of Cenozoic volcanism and Basin and Range extension in northwestern Nevada; New constraints from the northern Pine Forest Range: Geological Society of America Bulletin, v. 118, p. 126–139, doi: 10.1130/B25681.1.

Colgan, J.P., Dumitru, T.A., Reiners, P.R., Wooden, J.L., and Miller, E.L., 2006b, Cenozoic tectonic evolution of the Basin and Range Province in northwestern Nevada: American Journal of Science, v. 306, p. 616–654, doi: 10.2475/08.2006.02.

Colgan, J.P., John, D.A., and Henry, C.D., 2008, Large-magnitude Miocene extension of the Caetano caldera, southern Shoshone and northern Toiyabe Ranges, Nevada: Geosphere, v. 4, p. 107–130, doi: 10.1130/GES00115.1.

Dickinson, W.R., 2002, The Basin and Range Province as a composite extensional domain: International Geology Review, v. 44, p. 1–38.

Dilles, J.H., and Gans, P.B., 1995, The chronology of Cenozoic volcanism and deformation in the Yerington area, western Basin and Range and Walker Lane: Geological Society of America Bulletin, v. 107, p. 474–486, doi: 10.1130/0016-7606(1995)107<0474:TCOCVA>2.3.CO;2.

Egger, A.E., Dumitru, T.A., Miller, E.L., and Savage, C.F.I., 2003, Timing and nature of Tertiary plutonism and extension in the Grouse Creek Mountains, Utah: International Geology Review, v. 45, p. 497–532.

Ehlers, T.A., 2005, Crustal thermal processes and the interpretation of thermochronometer data: Reviews in Mineralogy and Geochemistry, v. 58, p. 315–350, doi: 10.2138/rmg.2005.58.12.

Ehlers, T.A., and Farley, K.A., 2003, Apatite (U-Th)/He thermochronometry; methods and applications to problems in tectonic and surface processes: Earth and Planetary Science Letters, v. 206, p. 1–14, doi: 10.1016/S0012-821X(02)01069-5.

Ehlers, T.A., Willet, S.D., Armstrong, P.A., and Chapman, D.A., 2003, Exhumation of the central Wasatch Mountains, Utah; 2, Thermokinematic model of exhumaton, erosion, and thermochronometer interpretation: Journal of Geophysical Research, v. 108, 2173, doi: 10.1029/2001JB001723.

Erwin, J.W., 1974, Bouguer gravity map of Nevada; Winnemucca Sheet Map: Nevada Bureau of Mines and Geology Report 47, scale 1:250,000, 1 sheet.

Farley, K.A., 2000, Helium diffusion from apatite: General behavior as illustrated by Durango Fluorapatite: Journal of Geophysical Research, v. 105, p. 2903–2914, doi: 10.1029/1999JB900348.

Farley, K.A., 2002, (U-Th)/He dating; techniques, calibrations, and applications: Reviews in Mineralogy and Geochemistry, v. 47, p. 819–843.

Faulds, J.E., and Varga, R.J., 1998, The role of accommodation zones and transfer zones in the regional segmentation of extended terranes, *in* Faulds, J.E., and Stewart, J.H., Accommodation zones and transfer zones; The regional segmentation of the Basin and Range Province: Geological Society of America Special Paper 323, p. 1–45.

Faulds, J.E., Feuerbach, D.L., Reagan, M.K., Metcalf, R.V., Gans, P., and Walker, J.D., 1995, The Mt. Perkins block, northwestern Arizona: An exposed cross section of an evolving, preextensional to synextensional magmatic system: Journal of Geophysical Research, v. 100, n. B8, p. 15,249–15,266.

Faulds, J.E., Henry, C.D., and Hinz, N.H., 2005, Kinematics of the northern Walker Lane: An incipient transform fault along the Pacific–North American plate boundary: Geology, v. 33, p. 505–508, doi: 10.1130/G21274.1.

Fitzgerald, P.G., Fryxell, J.E., and Wernicke, B.P., 1991, Miocene crustal extension and uplift in southeastern Nevada: Constraints from fission track analysis: Geology, v. 19, p. 1013–1016, doi: 10.1130/0091-7613(1991)019<1013:MCEAUI>2.3.CO;2.

Fonseca, J., 1988, The Sou Hills: A barrier to faulting in the Central Nevada Seismic Belt: Journal of Geophysical Research, v. 93, p. 475–489.

Fosdick, J.C., 2006, Miocene extension in the East Range: Documenting multiple episodes of normal faulting using low-temperature thermochronology [M.S. thesis]: Stanford, California, Stanford University, 60 p.

Foster, D.A., and John, B.E., 1998, Quantifying tectonic exhumation in an extensional orogen with thermochronology; examples from the southern Basin and Range Province: Geological Society [London] Special Publication 154, p. 343–364, doi: 10.1144/GSL.SP.1999.154.01.16.

Foster, D.A., Miller, D.S., and Miller, C.F., 1991, Tertiary extension in the Old Woman Mountains area, California: Evidence from apatite fission-track analysis: Tectonics, v. 10, p. 875–886.

Galbraith, R.F., and Laslett, G.M., 1993, Statistical models for mixed fission-track ages: Nuclear Tracks and Radiation Measurements, v. 21, p. 459–470, doi: 10.1016/1359-0189(93)90185-C.

Gleadow, A.J.W., Duddy, I.R., Green, P.F., and Lovering, J.F., 1986, Confined fission track lengths in apatite; A diagnostic tool for thermal history analysis: Contributions to Mineralogy and Petrology, v. 94, p. 405–415, doi: 10.1007/BF00376334.

Glen, J.M.G., and Ponce, D.A., 2002, Large-scale fractures related to inception of the Yellowstone hotspot: Geology, v. 30, p. 647–650, doi: 10.1130/0091-7613(2002)030<0647:LSFRTI>2.0.CO;2.

Goldstein, N.E., and Paulsson, B., 1978, Interpretation of gravity surveys in Grass and Buena Vista Valleys, Nevada: Geothermics, v. 7, p. 29–50, doi: 10.1016/0375-6505(78)90024-X.

Gonsior, Z.J., 2006, The timing and evolution of Cenozoic extensional normal faulting in the southern Tobin Range, Pershing County, Nevada [M.S. thesis]: Corvallis, Oregon State University, 52 p.

Gonsior, Z.J., and Dilles, J.H., 2008, The timing and evolution of Cenozoic extensional normal faulting in the southern Tobin Range, Nevada: Geosphere, in press.

Green, P.F., Duddy, I.R., Laslett, G.M., Hegarty, K.A., Gleadow, A.J.W., and Lovering, J.F., 1989, Thermal annealing of fission tracks in apatite: 4. Quantitative modeling techniques and extension to geological time scales: Chemical Geology, v. 79, p. 155–182.

Hastings, D.D., 1979, Results of exploratory drilling in northern Fallon Basin, western Nevada, *in* Newman, G.W., and Goode, H.D., eds., Basin and Range Symposium and Great Basin Field Conference: Denver, Rocky Mountain Association of Geology, p. 515–522.

Henry, C.D., 2008, Ash-flow tuffs and paleovalleys in northeastern Nevada: Implications for Eocene paleogeography and extension in the Sevier hinterland, northern Great Basin: Geosphere, v. 4, p. 1–35.

Henry, C.D., and Perkins, M.E., 2001, Sierra Nevada–Basin and Range transition near Reno, Nevada: Two-stage development at 12 and 3 Ma: Geology, v. 29, p. 719–722, doi: 10.1130/0091-7613(2001)029<0719:SNBART>2.0.CO;2.

Hudson, M.R., John, D.A., Conrad, J.E., and McKee, E.H., 2000, Style and age of late Oligocene–early Miocene deformation in the southern Stillwater Range, west central Nevada; Paleomagnetism, geochronology, and field relations: Journal of Geophysical Research, v. 105, p. 929–954, doi: 10.1029/1999JB900338.

Humphreys, E.D., 1995, Post-Laramide removal of the Farallon slab, western United States: Geology, v. 23, p. 987–990, doi: 10.1130/0091-7613(1995)023<0987:PLROTF>2.3.CO;2.

John, D.A., 1995, Tilted middle Tertiary ash-flow calderas and subjacent granitic plutons, southern Stillwater Range, Nevada: Cross sections of an Oligocene igneous center: Geological Society of America Bulletin, v. 107, p. 180–200, doi: 10.1130/0016-7606(1995)107<0180:TMTAFC>2.3.CO;2.

John, D.A., Wallace, A.R., Ponce, D.A., Fleck, R.B., and Conrad, J.E., 2000, New perspectives on the geology and origin of the Northern Nevada rift, *in* Cluer, J.K., et al., eds., Geology and ore deposits 2000: The Great Basin and beyond: Reno, Geological Society of Nevada, p. 127–154.

John, D.A., Henry, C.D., and Colgan, J.P., 2008, Magmatic and tectonic evolution of the Caetano caldera, north-central Nevada: A tilted mid-Tertiary eruptive center and source of the Caetano Tuff: Geosphere, v. 4, p. 75–106.

Ketcham, R.A., 2005, Forward and inverse modeling of low-temperature thermochronometry data: Reviews in Mineralogy and Geochemistry, v. 58, p. 275–314, doi: 10.2138/rmg.2005.58.11.

Lerch, D.W., Klemperer, S.L., Glen, J.M.G., Ponce, D.A., Miller, E.L., and Colgan, J.P., 2006, Crustal structure of the northwestern Basin and Range Province and its transition to unextended volcanic plateaus: Geochemistry Geophysics Geosystems, v. 8, Q02011, doi: 10.1029/2006GC001429.

McGrew, A.J., Peters, M.T., and Wright, J.E., 2000, Thermobarometric constraints on the tectonothermal evolution of the East Humboldt Range metamorphic core complex: Geological Society of America Bulletin, v. 112, p. 45–60, doi: 10.1130/0016-7606(2000)112<0045:TCOTTE>2.3.CO;2.

McQuarrie, N., and Wernicke, B.P., 2005, An animated tectonic reconstruction of southwestern North America since 36 Ma: Geosphere, v. 1, p. 147–172, doi: 10.1130/GES00016.1.

Metcalf, J.R., 2006, Constraining continental deformation with the apatite (U-Th)/He thermochronometer [Ph.D. thesis]: Stanford, California, Stanford University, 120 p.

Miller, E.L., Dumitru, T.A., and Brown, R.W., 1999, Rapid Miocene slip on the Snake Range–Deep Creek Range fault system, east-central Nevada: Geological Society of America Bulletin, v. 111, p. 886–905, doi: 10.1130/0016-7606(1999)111<0886:RMSOTS>2.3.CO;2.

Mueller, K.J., Cerveny, P.K., Perkins, M.E., and Snee, L.W., 1999, Chronology of polyphase extension in the Windermere Hills, Northeast Nevada: Geological Society of America Bulletin, v. 111, p. 11–27, doi: 10.1130/0016-7606(1999)111<0011:COPEIT>2.3.CO;2.

Nichols, K.M., and Silberling, N.J., 1977, Stratigraphy and depositional history of the Star Peak Group (Triassic), northwestern Nevada: Geological Society of America Special Paper 178, 73 p.

Nosker, S.A., 1981, Stratigraphy and structure of the Sou Hills, Pershing County, Nevada [M.S. thesis]: Reno, University of Nevada, 60 p.

Okaya, D.A., and Thompson, G.A., 1985, Geometry of Cenozoic extensional faulting; Dixie Valley, Nevada: Tectonics, v. 4, p. 107–125.

Parsons, T., Thompson, G.A., and Sleep, N.H., 1994, Mantle plume influence on the Neogene uplift and extension of the U.S. western Cordillera?: Geology, v. 22, p. 83–86, doi: 10.1130/0091-7613(1994)022<0083:MPIOTN>2.3.CO;2.

Pierce, L.A., and Morgan, K.L., 1992, The track of the Yellowstone hotspot: Volcanism, faulting, and uplift, *in* Link, P.K., et al., eds., Regional geology of eastern Idaho and western Wyoming: Geological Society of America Memoir 179, p. 1–53.

Proffett, J.M., Jr., 1977, Cenozoic geology of the Yerington District, Nevada, and implications for the nature and origin of Basin and Range faulting: Geological Society of America Bulletin, v. 88, p. 247–266, doi: 10.1130/0016-7606(1977)88<247:CGOTYD>2.0.CO;2.

Rahl, J.M., McGrew, A.J., and Foland, K.A., 2002, Transition from contraction to extension in the northeastern Basin and Range; New evidence from the Copper Mountains, Nevada: Journal of Geology, v. 110, p. 179–194, doi: 10.1086/338413.

Riehle, J.R., McKee, E.H., and Speed, R.C., 1972, Tertiary volcanic center, west-central Nevada: Geological Society of America Bulletin, v. 83, p. 1383–1395, doi: 10.1130/0016-7606(1972)83[1383:TVCWN]2.0.CO;2.

Silberling, N.J., 1975, Age Relationships of the Golconda Thrust Fault, Sonoma Range, north-central Nevada: Geological Society of America Special Paper 163, 28 p.

Smith, D.L., Gans, P.B., and Miller, E.L., 1991, Palinspastic restoration of Cenozoic extension in the central and eastern Basin and Range Province at latitude 39–40 degrees N, *in* Raines, G.L., et al., eds., Geology and ore deposits of the Great Basin: Reno, Geological Society of Nevada, p. 75–86.

Snow, J.K., and Wernicke, B.P., 2000, Cenozoic tectonism in the central Basin and Range: Magnitude, rate, and distribution of upper crustal strain: American Journal of Science, v. 300, p. 659–719, doi: 10.2475/ajs.300.9.659.

Speed, R.C., 1976, Geologic map of the Humboldt Lopolith and surrounding terrane, Nevada: Geological Society of America MC-14, scale 1:78740, 4 p., 1 sheet.

Stewart, J.H., 1980, Regional tilt patterns of late Cenozoic basin-range fault blocks, western United States: Geological Society of America Bulletin, v. 91, p. 460–464, doi: 10.1130/0016-7606(1980)91<460:RTPOLC>2.0.CO;2.

Stewart, J.H., and Carlson, J.E., 1978, Geologic map of Nevada: U.S. Geological Survey, scale 1:500,000, 2 sheets.

Stockli, D.F., 2005, Applications of low-temperature thermochronology to extensional tectonic settings: Reviews in Mineralogy and Geochemistry, v. 58, p. 411–448, doi: 10.2138/rmg.2005.58.16.

Stockli, D.F., Surpless, B.E., Dumitru, T.A., and Farley, K.A., 2002, Thermochronological constraints on the timing and magnitude of Miocene and Pliocene extension in the central Wassuk Range, western Nevada: Tectonics, v. 21, p. 289–307.

Stockli, D.F., Dumitru, T.A., McWilliams, M.O., and Farley, K.A., 2003, Cenozoic tectonic evolution of the White Mountains, California and Nevada: Geological Society of America Bulletin, v. 115, p. 788–816, doi: 10.1130/0016-7606(2003)115<0788:CTEOTW>2.0.CO;2.

Surpless, B.E., Stockli, D.F., Dumitru, T.A., and Miller, E.L., 2002, Two phase westward encroachment of Basin and Range extension into the northern Sierra Nevada: Tectonics, v. 21, p. 2–13.

Trexler, J.H., Cashman, P.H., Muntean, T., Schwartz, K., Ten Brink, A., Faulds, J.E., Perkins, M., and Kelly, T., 2000, Neogene basins in western Nevada document the tectonic history of the Sierra Nevada–Basin and Range transition zone for the last 12 Ma: Boulder, Colorado, Geological Society of America Field Guide, v. 2, p. 97–116.

Varga, R.J., Faulds, J.E., Snee, L.W., Harlan, S.S., and Bettison-Varga, L., 2004, Miocene extension and extensional folding in an anticlinal segment of the Black Mountains accommodation zone, Colorado River extensional corridor, southwestern United States: Tectonics, v. 23, TC1019, doi: 10.1029/2002TC001454.

Wallace, A.R., 1977, Geology and ore deposits, Kennedy mining district, Pershing County, Nevada [M.S. thesis]: Boulder, University of Colorado, 74 p.

Wallace, R.E., 1984, Patterns and timing of late Quaternary faulting in the Great Basin province and relation to some regional tectonic features: Journal of Geophysical Research, v. 89, p. 5763–5769.

Wells, M.L., Snee, L.W., and Blythe, A.E., 2000, Dating of major normal fault systems using thermochronology: An example from the Raft River detachment, Basin and Range, western United States: Journal of Geophysical Research, v. 105, p. 16,303–16,327, doi: 10.1029/2000JB900094.

Whitehill, C.S., Miller, E.L., Colgan, J.P., Dumitru, T.A., Lerch, D.W., McWilliams, M.O., 2004, Extent, style and age of Basin and Range faulting east of Pyramid Lake: Geological Society of America Abstracts with Programs, v. 36, n. 4, p. 37.

Wolf, R.A., Farley, K.A., and Silver, L.T., 1996, Helium diffusion and low-temperature thermochronometry of apatite: Geochimica et Cosmochimica Acta, v. 60, p. 4231–4240, doi: 10.1016/S0016-7037(96)00192-5.

Zeitler, P.K., Herczeg, A.L., McDougall, I., and Honda, M., 1987, U-Th-He dating of apatite; A potential thermochronometer: Geochimica et Cosmochimica Acta, v. 51, p. 2865–2868, doi: 10.1016/0016-7037(87)90164-5.

Zoback, M.L., McKee, E.H., Blakely, R.J., and Thompson, G.A., 1994, The northern Nevada rift: Regional tectono-magmatic relations and middle Miocene stress direction: Geological Society of America Bulletin, v. 106, p. 371–382, doi: 10.1130/0016-7606(1994)106<0371:TNNRRT>2.3.CO;2.

Manuscript Received 10 February 2007
Revised Manuscript Received 10 November 2007
Manuscript Accepted 16 December 2007

Printed in the USA